5

Remote-sensing science and technology for studying mountain environments

Michael P. Bishop, Jeffrey D. Colby, Jeffrey C. Luvall, Dale Quattrochi, and Douglas L. Rickman

5.1 INTRODUCTION

With new Earth-observing sensors in orbit and geographic information technology (GIT), Earth scientists have access to data and technology that can be used to assess mountain landscapes and system dynamics (Mather, 1992; Goward and Williams, 1997; Bishop et al., 1998b). Spatial analysis and modeling capabilities of geographic information systems (GISs) now enable scientists to study surface processes, feedback mechanisms, and landform-forcing factors at a variety of scales (Montgomery, 1994; Price and Heywood, 1994; Walsh et al., 1997; Bishop et al., 1998b; Bishop and Shroder, 2000; Finlayson and Montgomery, 2003). Consequently, geoscience and environmental investigations are increasingly utilizing satellite imagery, digital elevation models (DEMs), and spatial analysis and modeling techniques to study the spatial and temporal scale dependencies of surface processes and resources in mountains (Price and Heywood, 1994).

The availability of new data and technology, however, does not directly translate into accurate information for characterizing and understanding surface processes, environmental change, and mountain geodynamics. Information extraction from satellite imagery and spatial data sets is a complex problem (e.g., Danson et al., 1995). Although a few biophysical properties of the landscape can be directly or indirectly obtained from remotely sensed data (i.e., altitude, albedo, surface temperature, leaf area index), information extraction requires an understanding of radiation transfer processes as well as information science and technology solutions for characterizing and integrating spectral, spatial, and contextual information into application models.

A significant obstacle to studying mountain systems is quantitative characterization of the 3-D properties of the landscape and assessment of 3-D spatial and temporal relationships. From a remote-sensing perspective, topographic characterization is essential, because topography creates the problem of anisotropic

reflectance. Numerous environmental factors, such as the atmosphere, topography, and land cover, control surface irradiance and upward radiance. Other factors, such as solar and sensor geometry, must also be taken into consideration, such that the magnitude of surface-upwelling radiance varies in all directions (anisotropic reflectance). Consequently, satellite imagery must be radiometrically calibrated to account for these factors so that variations in image radiance are representative of the biophysical variations of the landscape.

From an applications perspective, numerous investigators have used and studied the efficacy of remote sensing and GIT for improving our understanding of mountain systems (e.g., Isacks, 1992; Burbank et al., 1996; Brozovik et al., 1997; Bishop et al., 1998b, 2002). Although much progress has occurred in the areas of land cover mapping and basic topographic analysis, much greater progress is required in terrain analysis, landform mapping, and geomorphological assessment and process modeling (Millington et al., 1995; Bishop and Shroder, 2000; Bishop et al., 2001, 2002). In general, the constraints have been lack of data, sensor characteristics (i.e., spatial and spectral resolution), and processing paradigms that are inappropriate for some problems and applications (e.g., per pixel image analysis and GIS grid cell analysis). New high-resolution imagery and DEMs, coupled with new developments in object-oriented modeling and analysis, artificial intelligence, geostatistics, spatial modeling, and 3-D analysis, offer new opportunities for assessing erosion (Bishop et al., 1995; Bishop and Shroder, 2000; Finlayson and Montgomery, 2003), landform mapping (Dikau, 1989; Brabyn, 1997; Blaszczynski, 1997), alpine glacier assessment (Aniya et al., 1996), snowmelt modeling (Bernhard and Weibel, 1999), and predicting environmental change caused by climate forcing (Halpin, 1994). These opportunities, however, can only be realized if Earth scientists address a variety of multidisciplinary issues.

The purpose of this chapter is to demonstrate the complexity of effectively utilizing satellite imagery to study mountains and to address technical and some application issues. We restrict our treatment of remote sensing to the solar reflective (0.4–3.0 μm) and thermal emission (3.0–14.0 μm) portions of the electromagnetic spectrum, although microwave and LIDAR (light detection and ranging) remote sensing are making significant contributions to DEM generation and to enabling other biophysical characteristics to be assessed and estimated for studying mountain landscapes (i.e., surface roughness, moisture content, canopy characteristics). We provide the background necessary for understanding the environmental information content in satellite imagery and address the problems associated with using imagery in rugged terrain. Technology-based solutions for radiometric calibration and anisotropic-reflectance correction are presented and discussed in the context of current research. Finally, we present an overview of mountain applications, provide specific examples, and discuss future research directions.

5.2 MISSIONS AND IMAGERY

A relatively short history exists for the utilization of images from space for geoscience studies. More than 150 investigations were funded by NASA in the

first 14 years of the Landsat program to evaluate and define the use of satellite imagery, primarily for geological applications. Comparable studies were undertaken using photography from such sources as the *Gemini*, *Apollo*, *Skylab*, and *Shuttle Orbiter* missions. These investigations focused on reconnaissance-level mapping, recognition of stratigraphic facies, rock-type discrimination, mapping of fractures and lineaments, the search for surficial indications of subsurface structure, detection of zones of hydrothermal alteration, analysis of regional tectonics, assessment of geologic hazards, and environmental geology (Short and Blair, 1986).

In contrast to aerial photographs, the primary advantage recognized for utilizing images from space was the synoptic or broad-area coverage that was possible, enabling entire mountain systems to be studied. The impact of multiple geomorphic processes operating over wide areas could be investigated from this perspective. Most studies, however, were primarily observational and descriptive in nature (Short et al., 1976; Short and Blair, 1986; Williams and Ferrigno, 1989).

The Committee on Earth Observation Satellites (CEOS) estimates that 40 Earth observation missions have been launched since 1984, and 50 more are planned in the next 15 years. In addition, several systems are planned for launch by the commercial sector. With the suite of current and planned satellite sensors in orbit, terabytes of data depicting the Earth's surface will become available on a daily basis. A variety of applications will benefit from the wealth of data acquired from these sensors, including geomorphic studies in mountain environments. These sensors have been developed through the efforts and often collaboration of a number of countries, and represent a wide range of spectral and spatial resolutions. Examples of some of the satellites and sensors are described in Table 5.1.

The Landsat program is the longest running, remote-sensing program from space, accounting for over 29 years of data collection. The Landsat series began with the launch of the Earth Resources Technology Satellite (*ERTS-1*) in 1972. Recently, *Landsat 4* and *5* have been decommissioned due to the high cost of operation. *Landsat 6* failed to achieve orbit in 1993. *Landsat 7* was launched on 15 April 1999. *Landsat 7* includes the Enhanced Thematic Mapper (ETM) instrument. Innovations on the ETM include a panchromatic band with 15 m spatial resolution and a thermal infrared channel with 60 m resolution. Recent geomorphic applications in mountain environments reflect the topical trend of early studies—for example, the mapping of glaciers and the spatial distribution of snow and its characteristics (e.g., Allen, 1998; Cline et al., 1998; Fily et al., 1999), mapping volcanic surfaces and natural hazards (Flynn et al., 2001), reconstruction of glacial terrains (Smith et al., 2000), and mapping alluvial geomorphic features (Beratan and Anderson, 1998).

The SPOT (Satellite Pour l'Observation de la Terre) program, with over 7.5 million archived images, represents another important source of remotely sensed data for Earth surface observations. Through the cooperation of the French Space Agency CNES (Centre National d'Etudes Spatiales) and Belgium and Sweden, the SPOT Image Corporation was created in 1982 as the first commercial company established to distribute remotely sensed data. The system consists of three satellites that are currently transmitting data, *SPOT 2*, *3*, and *4*. *SPOT 2* and *3* carry two

Table 5.1. Missions suitable for mountain applications.

Mission	Launch	Instruments	Wavebands	Spectral/spatial resolution (m)				Swath (km)	Stereo
				PAN	VNIR	SWIR	TIR		
Landsat 4	1982	MSS	4		80			185	
		TM	7		30	30	120	185	
Landsat 5	1984	MSS	4		79			185	
		TM	7		30	30	120	185	
Landsat 7	1999	ETM	8	15	30	30	60	185	
SPOT 2	1990	HRV	4	15	20			60	•
SPOT 3	1993	HRV	4	15	20			60	•
SPOT 4	1998	HRV-IR	5	10	20	20		60	•
Resurs-O1-3 and *4*	1994 and 1998	MSU-E	3		45			45–58	• ±30°
		MSU-SK	5		160		600	600–710	
IRS-IC and *ID*	1995 and 1997	LISS-3	3		23			142	
		PAN	1	5.8				70	•
		WiFS	2		188			774	
IRS-P3	1996	MOS	18		520	520		200	
		WiFS	3		188	188		774	
IRS-P5	2003	PAN		2.5					•
Ikonos	1999		5	1	4			11	
Terra (EOS AM-1)	1999	ASTER	14		15	30	90	60	•
		MISR	4		275			360	
		MODIS	36		250/500/1,000	500/1,000	1,000	2,330	• ±55°
Quickbird 2	2001		5	0.61	2.44			16.5	• ±30°
ADEOS-II	2002	GLI	36		250/1,000	250/1,000	1,000	1,000	• ±20°

		MODIS	36		250/500/1,000	500/1,000	1,000	2,330	• ±55°
Quickbird 2	2001		5	0.61	2.44			16.5	• ±30°
ADEOS-II	2002	GLI	36		250/1,000	250/1,000	1,000	1,000	• ±20°

high-resolution visible (HRV) sensors and *SPOT 4* carries two high-resolution, visible infrared (HRV-IR) sensors. The HRV and HRV-IR sensors are pointable (up to 27° off-nadir) which enables the acquisition of stereoscopic imagery and the capability of developing DEMs. The planned *SPOT 5* sensor, the high-resolution geometry (HRG), will provide higher ground resolution in both the panchromatic (2.5 m and 5 m) and multispectral modes (10 m). SPOT imagery has been used for snow cover mapping and the assessment of hydrologic units (Haefner et al., 1997) and for geologic mapping (Saintot et al., 1999; Sung and Chang, 2000).

The flagship satellite for NASA's Earth Observation System (EOS) program is *Terra*. The *Terra* satellite, originally known as *EOS AM-1*, was successfully launched in December 1999. One of the primary science objectives of the *Terra* program is to study the changing global land surface. Three of the sensors on *Terra* are of particular interest to geoscientists. The first is the advanced spaceborne thermal emission and reflection (ASTER) radiometer instrument, which obtains high-resolution images (15–90 m) at 14 different wavelengths. The ASTER data will be used to map surface temperature, reflectance, emissivity, and altitude and will provide high spatial resolution data to be compared with the coarser resolution data obtained by other *Terra* sensors. The multiangle imaging spectroradiometer (MISR) acquires reflectance values in three visible and one near-infrared band at a resolution of 275 m. A unique characteristic of the MISR sensor is that it acquires data from cameras pointed in nine directions, which is designed to enable study of the scattering of sunlight in different directions under natural conditions, and improve the characterization of clouds, aerosol particles, and land cover. The moderate resolution spectroradiometer (MODIS) collects data for 36 spectral bands at spatial resolutions from 250 to 1,000 m and will view the entire surface of the Earth every 1–2 days. MODIS will be used to make observations of land surface cover, primary productivity, land and ocean surface temperature, aerosols, water vapor, clouds, temperature profiles, and fires.

The *Ikonos* satellite, launched in September of 1999 by Space Imaging Inc., is the first of a new generation of high-resolution commercial satellites. The imagery will complement the broad-area coverage of lower resolution satellite data and very high-resolution aerial imagery. *Ikonos* utilizes a pushbroom imaging system that provides images at 1 m (panchromatic) and 4 m (multispectral) resolutions. Accuracy requirements for medium-scale topographic mapping (1 : 10,000–1 : 24,000) can be met using 1 m resolution imagery.

Other countries have launched additional series of satellites, notably in Europe, and by India, Russia, and Japan. The Indian Remote Sensing (IRS) satellite program has four satellites in orbit, at the time of writing. This program was developed to provide the capability for groundwater exploration, surface water inventory, and land use, forest, and flood mapping. Perhaps the most widely available data is obtained from the *IRS-1C* and *IRS-1D* sensors launched in 1995 and 1997, respectively. These sensors provide 5 m panchromatic data and 25 m multispectral data. Snow studies and geological mapping for identifying mineral sites are two of the primary applications for data obtained from the *IRS-P3* satellite, launched in 1996.

The anticipated launch of *IRS-P5*, designed for cartographic mapping purposes, will provide high-resolution panchromatic imagery at 2.5 m resolution.

In general, the nature of remote-sensing investigations have not significantly evolved from the early qualitative studies, despite the tremendous volume of new data and improved quality. This is slowly changing as geoscientists now have new models and tools for image calibration and biophysical information extraction.

5.3 RADIATION TRANSFER

Extracting accurate information from satellite imagery in mountainous terrain is problematic (Hugli and Frei, 1983). Numerous factors other than the biophysical characteristics of the landscape influence the magnitude of incoming and reflected radiation. Consequently, satellite imagery must be radiometrically calibrated to account for atmospheric, topographic, and landscape effects.

Addressing the problems of anisotropic reflectance requires an understanding of radiation transfer processes. Topography plays a significant role, although its influence has not been accurately characterized (Smith et al., 1980; Hugli and Frei, 1983; Proy et al., 1989).

The magnitude of exoatmospheric irradiance (E_λ^0) at the top of the Earth's atmosphere is a function of the spectral exitance of the sun (M_λ) and the distance between the Earth and the Sun. The total spectral irradiance at the Earth surface (E_λ) is a composite of three components such that:

$$E_\lambda = E_\lambda^h + E_\lambda^d + E_\lambda^t \tag{5.1}$$

where E_λ^h is the direct-beam irradiance component, E_λ^d is the diffuse-skylight irradiance component, and E_λ^t is the adjacent-terrain irradiance component.

5.3.1 Direct solar irradiance

The atmosphere attenuates direct irradiance primarily by gaseous absorption and molecular and aerosol scattering (Chavez, 1996). These atmospheric processes are wavelength-dependent and spatially controlled by the constituents and properties of the atmosphere. Therefore, atmospheric transmission ($\tau_\lambda^\downarrow$) is a function of the total optical depth of the atmosphere, such that for a horizontal surface, $E_\lambda^h = E_\lambda^0 \tau_\lambda^\downarrow$. The optical depth of the atmosphere is spatially variable depending on the hypsometry of the landscape (i.e., altitude–area distribution). In many mountain ranges, extreme relief dictates significant changes in $\tau_\lambda^\downarrow$ over relatively short horizontal distances.

It is necessary to account for local illumination conditions that vary as a function of solar geometry and local topographic parameters. Local topographic conditions are accounted for by calculating the incidence angle of illumination (i) between the Sun and the vector normal to the ground, such that:

$$\cos i = \cos\theta_s \cos(\beta_t) + \sin\theta_s \sin\beta_t \cos(\phi_t - \phi_s) \tag{5.2}$$

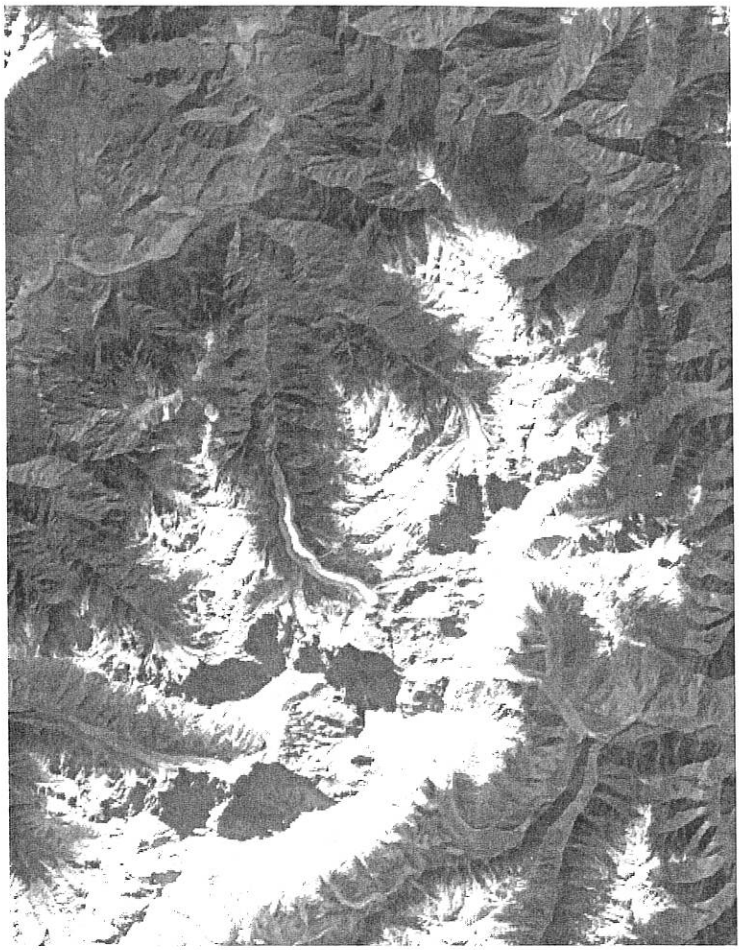

Figure 5.1. *SPOT 2* HRV panchromatic image of Nanga Parbat in northern Pakistan. Image acquisition date is 31 October 1991 at 06:05:08 UMT, with θ_s and ϕ_s values of 50.2° and 167.5°, respectively. Direct irradiance variations (cast shadows) make it difficult to use the imagery for mapping or biophysical applications. Image width is approximately 40 km and north is toward the top of the page.

where θ_s is the solar zenith angle, ϕ_s is the solar azimuth angle, β_t is the slope angle of the terrain, and ϕ_t is the slope–aspect angle of the terrain.

Calculation of $\cos i$ is possible with the use of a DEM, and $\cos i$ values can be ≤ 0.0, indicating no direct irradiance due to the orientation of the topography. The surrounding topographic relief is not accounted for by equation (5.2), and the altitude distribution in the direction of ϕ_s must be considered to determine whether a pixel is in shadow (S). Satellite imagery acquired in rugged terrain with relatively high, solar zenith angles exhibit cast shadows (Figure 5.1). This can be addressed by ray tracing, shadow detection, and shadow interpolation algorithms

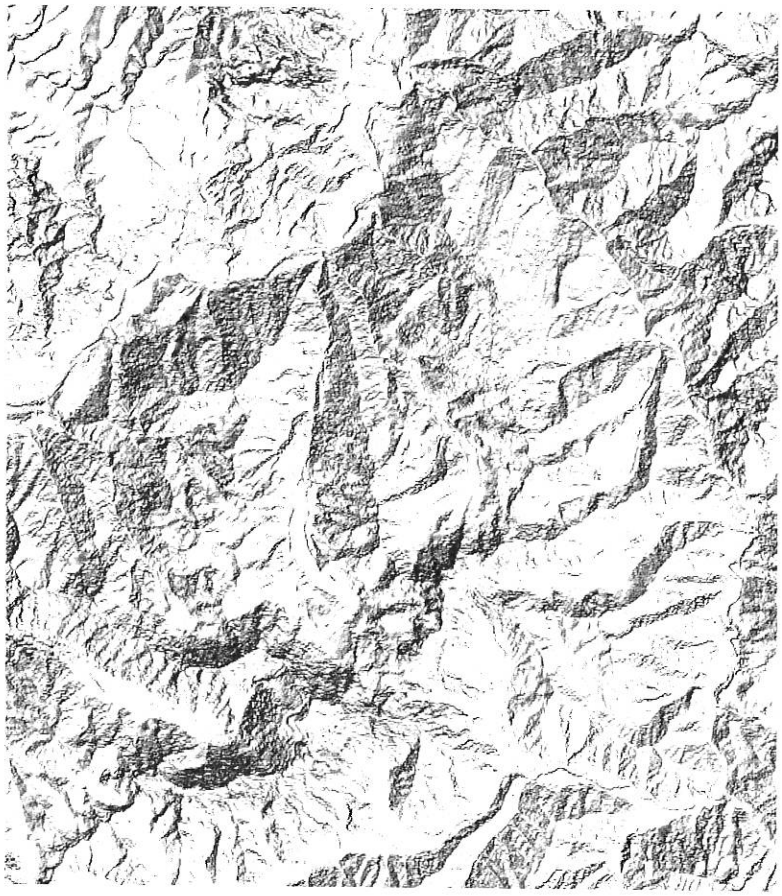

Figure 5.2. The spatial distribution of simulated direct irradiance (E_λ^h) over the Nanga Parbat Massif (2,150 km^2) in the near-infrared region of the spectrum (0.79–0.89 μm). Local topographic variations (slope and slope aspect) are primarily responsible for irradiance variation. Lighter grey tones represent higher direct irradiance. The image size is ~40 × 50 km, and north is toward the top of the page.

that alter cos i values appropriately (Dozier et al., 1981; Rossi et al., 1994; Giles, 2001). The local topography and cast shadows increase the global variance in satellite images, with a decrease in spectral variance associated with shadowed areas. The direct irradiance component can be defined as:

$$E_\lambda^h = E_\lambda^0 \tau^\downarrow \lambda \cos i S \tag{5.3}$$

and can be highly variable over the landscape (Figure 5.2).

5.3.2 Diffuse skylight irradiance

Atmospheric scattering will produce a hemispherical source of irradiance (E_λ^d; Figure 5.3). This source is composed of a direct downward-skylight component

the Nanga Parbat
)–0.89 μm). Local
ole for irradiance
ie image size is

al., 1994; Giles,
bal variance in
with shadowed

(5.3)

irradiance (E_λ^d;
ight component

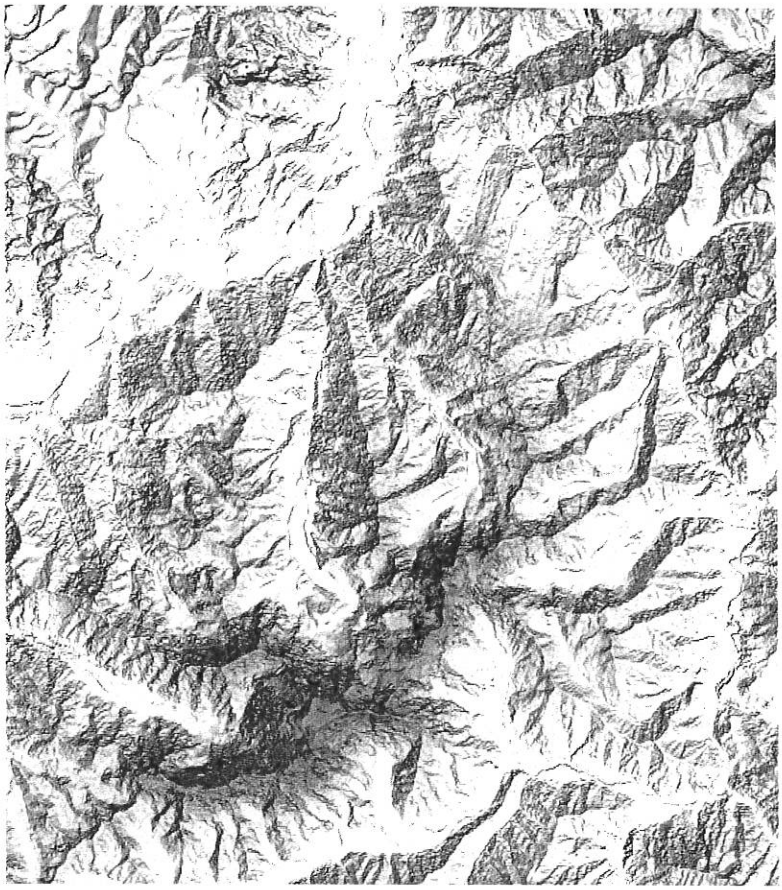

Figure 5.3. The spatial distribution of simulated diffuse-skylight irradiance (E_λ^d) over the Nanga Parbat Massif (2,150 km^2) in the near-infrared region of the spectrum (0.79–0.89 μm). Mesoscale topographic shielding causes irradiance variations, such that the large Indus Valley (upper northwestern portion of the image) exhibits relatively high E_λ^d values due to reduced shielding and flat topography. Basin ridge tops also receive more diffuse irradiance than valley walls. Lighter grey tones represent higher diffuse irradiance. The image size is ~40 × 50 km, and north is toward the top of the page.

and a diffuse component caused by multiple interactions between the ground surface and the atmosphere (Iqbal, 1983; Proy et al., 1989). It is represented as:

$$E_\lambda^d = \int_{\phi=0}^{2\pi} \int_{\theta=0}^{\pi/2} L(\theta_s, \theta_a, \phi_a) \cos i \sin\theta \, d\theta \, d\phi \tag{5.4}$$

where L is the downward radiance at the bottom of the atmosphere and θ_a and ϕ_a represent the atmospheric zenith and azimuth direction angles, respectively.

Investigators have attempted to estimate E_λ^d based on the simple relationship $E_\lambda^d = E_\lambda^h g$, where E_λ^h is the diffuse irradiance for a horizontal surface and g

represents a parameter that takes into consideration the local slope of the terrain (Temps and Coulson, 1977). Hemispherical shielding of the topography must be considered, however, as a significant part of the hemisphere can be masked by topography. Consequently, only a solid angle of the sky will contribute to E_λ^d, and this angle will change as a function of pixel location and direction. In general, the solid angle will increase with altitude. In mountain environments exhibiting extreme relief and deep valleys, topographic shielding of the solar diffuse irradiance can be significant (Proy et al., 1989).

5.3.3 Adjacent terrain irradiance

The irradiance components E_λ^b and E_λ^d interact with the terrain to represent an adjacent-terrain irradiance component (E_λ^t) which is a function of topography and land cover.

A first-order approximation to this irradiance component has been formulated by Proy et al. (1989) which assumes that surface radiance is Lambertian (magnitude of reflectance is equal in all directions). It is possible to estimate the radiance received at any pixel by accounting for the geometry between two pixels (p_1 and p_2) such that:

$$L_{12} = \cos\theta_1 \left(L_2 \cos\theta_2 \left[\frac{A}{d_{12}^2} \right] \right) \tag{5.5}$$

where L_{12} represents the radiance received at p_1 from the luminance of $p_2(L_2)$, θ_1 and θ_2 are the angles between the normal to the terrain and the direct line of sight from p_1 to p_2, A is the area of pixel p_2, and d_{12} represents the distance between p_1 and p_2.

With this equation we can estimate E_λ^t for any pixel by summing all of the pixels whose slopes are oriented toward a pixel of interest and where the line of sight is not blocked by topography. Therefore:

$$E_\lambda^t = \sum_{\phi=0}^{360} \sum_{i=1}^{d_{\max}} L_{\phi,i} \tag{5.6}$$

where ϕ represents the azimuth angle to account for the adjacent terrain, and i represents the distance from p_1 in the direction of ϕ. Extreme local relief areas can exhibit a strong adjacent-terrain irradiance component (Figure 5.4).

5.3.4 Surface radiance

The magnitude of the reflected and emitted radiance at the surface is determined by the conservation of energy, such that:

$$\rho_\lambda + \alpha_\lambda + \tau_\lambda = 1.0 \tag{5.7}$$

where ρ, α, and τ represent reflectance, absorption, and transmission, respectively. For opaque objects ($\tau = 0.0$), α is equivalent to the emissivity (ε_λ) of the object,

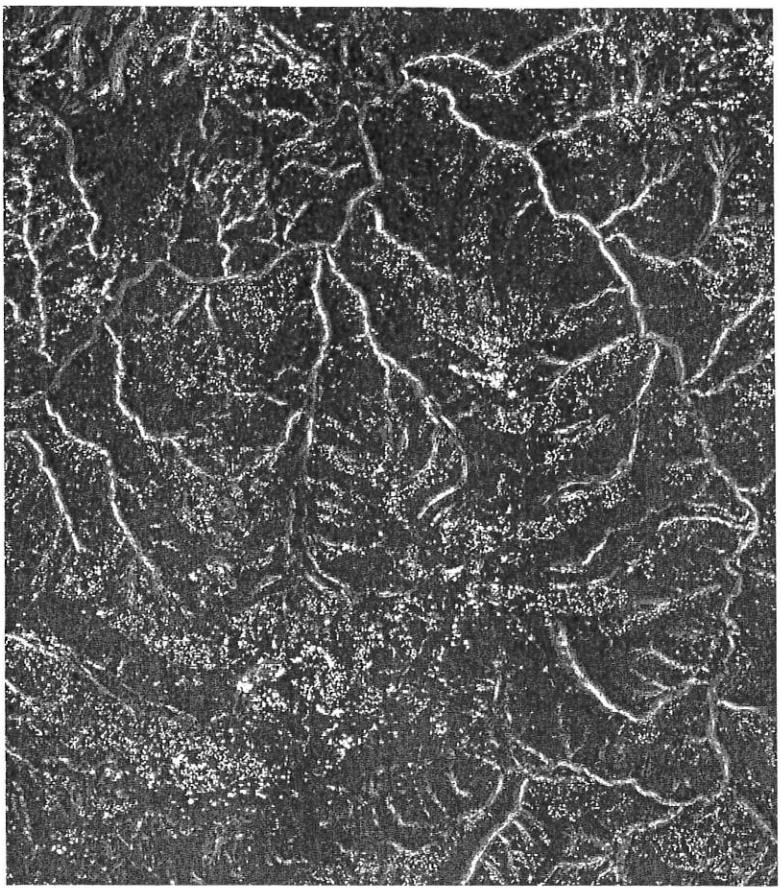

Figure 5.4. The spatial distribution of simulated adjacent-terrain irradiance (E_λ^t) over the Nanga Parbat Massif (2,150 km^2) in the near-infrared region of the spectrum (0.79–0.89 μm). Hemispherical analysis of the adjacent terrain was performed over a 1 km radius for each pixel. Grey tones represent the relative magnitude of E_λ^t values, with relatively higher irradiance associated with V-shaped valleys cut by incising rivers. DEM error is responsible for the random point distribution of irradiance. The image size is ~ 40 × 50 km, and north is toward the top of the page.

which describes how well the object radiates energy. Therefore, spectral reflectance can be represented as:

$$\rho_\lambda = \frac{M_\lambda}{E_\lambda} \tag{5.8}$$

where M_λ represents the spectral exitance at the surface given the conversion of incident flux to thermal energy as determined by α. The reflected radiance can be computed as follows:

$$L_\lambda = \rho_\lambda \left(\frac{E_\lambda}{\pi} \right) \tag{5.9}$$

where L_λ is the upward radiance from the landscape. Equation (5.9) represents the Lambertian reflectance assumption. We know, however, that this assumption is not valid in alpine environments due to the topography and biophysical characteristics of the landscape (Smith et al., 1980; Kimes and Kirchner, 1981; Hugli and Frei, 1983; Hall et al., 1988; Dozier, 1989; Aniya et al., 1996; Greuell and de Ruyter de Wildt, 1999).

Similarly, in the thermal region of the spectrum the emitted radiance can be represented as follows:

$$L_\lambda = \varepsilon_\lambda \left(\frac{M_\lambda(T)}{\pi} \right) \tag{5.10}$$

Scientists usually assume that emissivity or temperature (T) is spatially constant, although it is known that emissivity can vary with wavelength and temperature. In addition, spectral emissivity is generally not well known and can be highly variable over the land surface (Thorne et al., 1998).

Given the complex nature of radiation transfer in mountain environments, a considerable amount of research is ongoing to characterize the bidirectional reflectance distribution function (BRDF), which describes the magnitude of reflectance for all combinations of input–output angles. For example, Greuell and de Ruyter de Wildt (1999) measured numerous BRDFs for melting glacier ice in Switzerland. They found that all BRDFs exhibited similar patterns and that the amount of anisotropy increased with an increase in wavelength, with increasing solar zenith angle, and decreasing albedo. Other researchers have investigated alpine snow and vegetation canopies (Dozier, 1989; Jacquemoud et al., 2000). Unfortunately, the BRDF is very difficult to measure accurately, especially on inclined surfaces, and more research is required to understand the interactions between bidirectional reflectance, topography, and land cover conditions.

The upwelling surface radiance will then be altered by the atmosphere. Much research has documented the multiplicative and additive influences of the atmosphere, as attenuation and additive path radiance dictates the irradiance recorded by a sensor (Kawata et al., 1988; Chavez, 1989, 1996; Thorne et al., 1998). This complexity dictates that special emphasis be given to radiometric calibration of satellite data before it can be utilized.

5.4 RADIOMETRIC CALIBRATION

Given a variety of application objectives, it is essential that satellite imagery be accurately radiometrically calibrated so that multispectral and multitemporal data can be used effectively. Unfortunately, unlike geometric calibration, accurate radiometric calibration of satellite imagery is problematic due to complex surface–atmosphere interactions (Kimes and Kirchner, 1981; Chavez, 1989; Thorne et al., 1998). In general, radiometric calibration involves:

- conversion of image digital numbers (DNs) to at-satellite radiance values;

- atmospheric correction to remove the influence of atmospheric attenuation and additive path radiance;
- anisotropic-reflectance correction to modify radiance values to account for bidirectional reflectance caused by topography and land cover.

A DN-to-radiance conversion represents a linear transformation that is applied to every pixel. The transformation makes use of pre-launch or post-launch calibration coefficients and removes the gain and offset effects introduced by the sensor. For example, Chavez (1996) used the relationship $L_\lambda^0 = DN_\lambda - \alpha_o)/\alpha_g$ to transform DNs of *Landsat*'s Thematic Mapper (TM) to at-satellite radiance, where α_o and α_g represent the system offset and gain effects of the sensor, respectively. For *SPOT-1* HRV data the relation between spectral radiance and DNs is $DN_\lambda = \alpha_\lambda L_\lambda$, where L is the *SPOT* equivalent radiance and α_λ is an absolute calibration coefficient (Yang and Vidal, 1990). Other satellite sensors have similar linear transformations that convert digital numbers to at-satellite radiance based on the gain settings of the sensor. This initial calibration procedure is necessary in quantitative studies as spectral characteristics can be significantly distorted by system gain and offset conditions (Chavez, 1996).

Atmospheric correction

At-satellite radiance (L_λ^0) values require further modification to account for the influence of the atmosphere. Specifically, the additive effects and attenuation can significantly influence results involving estimation of surface parameters (reflectance and albedo), signature extension, classification of spectral signature, change detection, and comparisons between sensors (Chavez, 1989, 1996; Conese et al., 1993a).

Numerous atmospheric correction models for images have been developed for remote-sensing applications, and they enable the estimation of surface radiance (L_λ), such that:

$$L_\lambda = (L_\lambda^0 - L_\lambda^p)/\tau_\lambda^\uparrow(\theta_v)$$

where L_λ^p represents the additive path-radiance component caused by the scattering of the direct beam component into the sensor field of view, $\tau_\lambda^\uparrow$ is the beam transmittance of the atmosphere in the upward direction, and θ_v is the view angle of the sensor. The atmospheric transmission is a function of the molecular optical thickness (τ_m), ozone optical thickness (τ_o), aerosol optical thickness (τ_a), and moisture optical thickness (τ_{H_2O}) (Iqbal, 1983; Conese et al., 1993b). For a horizontal surface and nadir viewing, transmission can be approximated by $\tau^\uparrow = \exp(-\tau_o - \tau_m - \tau_a)$.

Accurate estimates of L_λ^p and $\tau_\lambda^\uparrow$ require knowledge of the state of the atmosphere at the time of image acquisition. This information is generally not available and has prompted researchers to take different approaches in estimating atmospheric parameters. In general, they include:

- Sky reflectance method. *In situ* measurements are recorded by a radiometer which records the sky irradiance at the time of acquisition.

- Satellite imagery method. This approach uses satellite data from sensors like the MISR and MODIS for estimating atmospheric parameters (Thorne et al., 1998). This requires that additional satellite data be acquired for the same area and time.
- Atmospheric correction models. Complex atmospheric models are used to estimate the influence of scattering and absorption for atmospheric correction (Chavez, 1996; Richter, 1997; Vermote et al., 1997). Some models, for example, make use of standard atmospheres and look-up tables to permit atmospheric correction.
- Dark object subtraction methods. Empirical techniques have been used to estimate L'_λ to receive a first-order approximation to atmospheric correction (Chavez, 1988, 1989).

Mountain topography significantly influences radiative transfer, such that accurate atmospheric correction also involves accounting for altitude and first and second-order topographic parameters (Dozier, 1989; Proy et al., 1989). For mountains that exhibit extreme relief, optical depth variations must be considered and dark object subtraction methods may not produce reasonable results.

Anisotropic reflectance correction

Earth scientists working in mountains must correct for the influence of topography on spectral response. The literature refers to this as the removal or reduction of the *topographic effect* in satellite imagery, although it is also directly related to atmospheric corrections. Radiometric calibration to accomplish this is generally referred to as *topographic normalization* (e.g., Civco, 1989; Colby, 1991; Conese et al., 1993b).

The nature of the problem, however, is extremely complex, as at-satellite radiance is governed by radiative transfer interactions between atmosphere, topography, land cover spatial structure, and biophysical properties (Proy et al., 1989; Yang and Vidal, 1990). Consequently, the problem is one of anisotropic-reflectance correction (ARC), as all of the aforementioned environmental factors dictate the characteristics of the BRDF and the magnitude of the radiance recorded by the sensor. From an applications point of view, ARC is required to accurately map mountain landscapes and estimate important biophysical parameters.

Research into ARC has been ongoing for about 20 years. To date, an operational model or procedure to meet the needs of Earth scientists has yet to emerge, although progress is being made. In general, scientists have taken a variety of approaches to reduce spectral variability caused by topography. These approaches include:

- Spectral feature extraction. Various techniques are applied to the original images and new spectral feature images are used for subsequent analysis. This includes the integration of DEMs into empirical analysis procedures.
- Empirical modeling. Empirical equations are developed by characterizing reflectance and topography relationships within a particular scene. Normalizing equations are typically generated using regression analysis.

- Semi-empirical modeling. The influence of topography on spectral response is physically modeled using topographic parameters, and $\cos i$ is generally considered to be proportional to E_λ^h.
- Physical radiative transfer models. Various components of the radiative transfer process are modeled.

The different approaches have their advantages and disadvantages with respect to ARC, computation, radiometric accuracy, and application suitability. Spectral feature extraction and the use of spectral band ratios and principal components analysis (PCA) have been adopted by a variety of investigators (Holben and Justice, 1981; Conese et al., 1993c; Ekstrand, 1996). Research indicates that spectral band ratioing and PCA can be used to produce spectral features that reduce the influence of the topographic effect. The limitations of this approach are in the empirical nature of the results such that they are scene-dependent. Furthermore, there are radiometric and technical issues that must be considered.

For example, spectral band ratioing has been found to reduce the topographic effect (Kowalik et al., 1983; Ekstrand, 1996). It is important, however, to account for such atmospheric effects as the additive path-radiance term before ratioing (Kowalik et al., 1983). This dictates that DN values must be converted to radiance and that atmospheric correction procedures account for optical depth variations. Only in this way can a reasonable first-order approximation to atmospheric correction be obtained in extreme relief areas. In addition, information may be lost in areas where cast shadows are present.

One might also expect that ratioing using visible bands may not be effective due to the influence of the atmosphere. Ekstrand (1996) found this to be the case and indicated that the blue and green spectral bands of TM data should not be used in ratios to remove the topographic effect. Therefore, depending on topographic conditions and time of image acquisition, spectral ratioing and PCA may or may not be useful for thematic mapping. For biophysical remote-sensing applications, however, ratioing and PCA do not address the problem.

A number of investigations have attempted to reduce the topographic effect by accounting for the nature of surface reflectance (Lambertian or non-Lambertian) and the local topographic conditions (e.g., Colby, 1991; Ekstrand, 1996; Colby and Keating, 1998). Semi-empirical approaches make use of a DEM to account for the local illumination conditions for each pixel and may assume isotropic upward radiance. Given this assumption, the cosine law correction can be used as follows:

$$L_\lambda^n = \frac{L_\lambda}{\cos i} \tag{5.12}$$

where L_λ^n represents the normalized radiance, L_λ represents the surface radiance, and $\cos i$ is defined by equation (5.2).

Research findings indicate that this approach may produce reasonable results for terrain where slope angles and solar zenith angles are relatively low (Smith et al., 1980), although numerous investigators have found that this approach does not work well in more complex topography as overcorrection occurs (Figure 5.5),

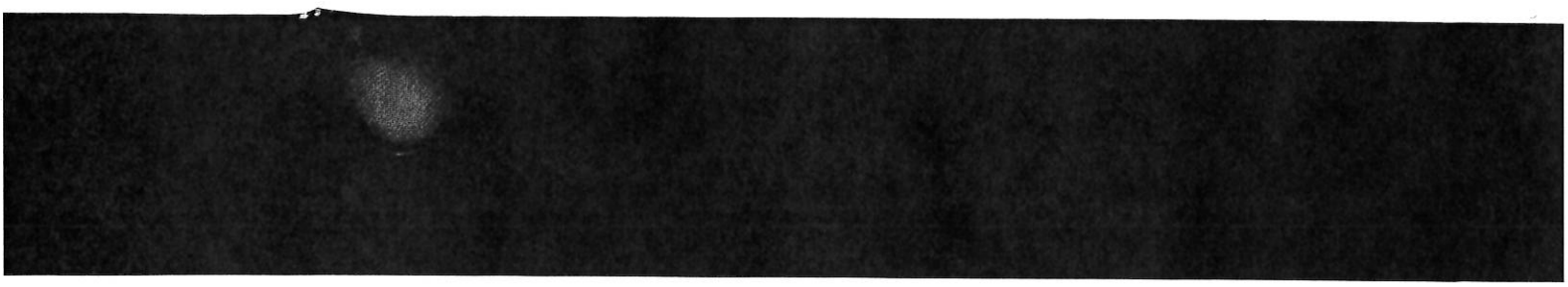

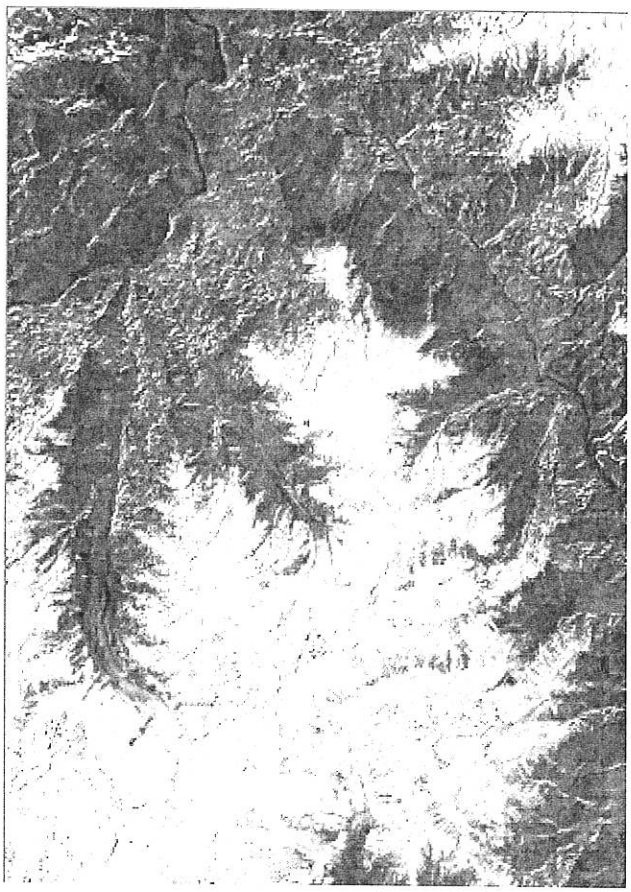

Figure 5.5. *SPOT-3* HRV NIR image of Nanga Parbat after topographic normalization using the cosine correction method. High radiance values are found throughout the image (light gray tones) at all altitudes where steep slopes reduce direct solar irradiance, and contributions from diffuse skylight and adjacent terrain irradiance are not accounted for. The image size is $\sim 30 \times 40$ km, and north is toward the top of the page.

producing an inverse topographic effect (Civco, 1989; Bishop and Colby, 2002). This result can be attributed to not accounting for the diffuse-skylight and adjacent-terrain irradiance components, which can significantly affect surface radiance (Proy et al., 1989). Consequently, many investigators have turned to the Minnaert correction procedure, which assumes anisotropic reflectance.

The Minnaert correction procedure has been used by a variety of investigators to reduce the topographic effect in imagery (e.g., Colby, 1991; Ekstrand, 1996; Bishop et al., 1998b; Colby and Keating, 1998). The correction procedure makes use of the Minnaert constant k, such that:

$$L_\lambda^n = L_\lambda(\cos e)/(\cos^k i \cos^k e) \tag{5.13}$$

where L_λ^n is normalized radiance, L_λ is surface radiance, and e is exitance angle ($e = \beta_t$ for nadir viewing). As shown here, k represents a globally-derived dimensionless coefficient that is wavelength-dependent and ranges from 0.0 to 1.0. It is empirically calculated using least-squares regression on the variables x and y, where $x = \log(\cos i \cos e)$ and $y = \log(L_\lambda \cos e)$. The slope of the regression equation represents k. The correction procedure defaults to the Lambertian assumption when $k = 1.0$.

Although this procedure reduces the topographic effect in imagery, the use of one globally-derived k value does not characterize the variability of anistropy caused by topography and land cover in complex environments (Bishop and Colby, 2002). Ekstrand (1996) found the use of one fixed k value to be inadequate in a study in southwestern Sweden, and initial studies indicated that a unique k value may be needed for each land cover class (Estes, 1983). Colby (1991) and Colby and Keating (1998) indicated that locally derived k values might address this problem.

In the western Himalaya, Bishop and Colby (2002) compared methods and implementations of the Minnaert correction procedure. They demonstrated that usable globally-derived and locally-derived k values are difficult to compute given the complexity of land cover conditions in alpine environments. They also found overcorrected normalized radiance values at the base of steep slopes, where the direct irradiance component does not accurately represent the magnitude of the surface irradiance (Figure 5.6). It is important to note that ARC procedures can alter the spatially dependent variance structure of satellite imagery (Bishop and Colby, 2002). Consequently, the visual appearance of reduced spectral variation does not mean that the scene has been accurately radiometrically calibrated. These findings indicate that the Minnaert correction procedure has the potential to be used to address this problem, although software to compute accurate k values is generally not available and the other irradiance components may need to be included in the analysis.

This has prompted many scientists to develop and evaluate empirical corrections that are based on the relationship between at-satellite or surface radiance and the topography. For example, Civco (1989) used a two-stage approach to reduce the topographic effect in *Landsat* TM data. The first stage was based on statistics from an illumination model, while the second stage utilized an empirical calibration coefficient to alter first-stage results. Others have evaluated the use of correction coefficients for altering the Minnaert constant (Teillet et al., 1982; Meyer et al., 1993). These and other empirical approaches have helped Earth scientists receive acceptable results for various applications given scene characteristics. It should be noted, however, that empirical procedures are not suitable for operational ARC, which will be increasingly needed for planetary geoscience projects.

The ideal situation is to develop physical radiative transfer models that account for multiple interactions at altitude. Such models at the appropriate scale are not available, as accurate parameter estimates are not available, and this would require a significant amount of computational resources (Hugli and Frei, 1983; Yang and Vidal, 1990). Progress has been made in modeling various components of the transfer process (e.g., Proy et al., 1989; Vermote et al., 1997), although modeling software that integrates satellite imagery is not readily available. More research and

rmalization using
the image (light
and contributions
The image size is

lby, 2002). This
t and adjacent-
irface radiance
o the Minnaert

investigators to
d, 1996; Bishop
nakes use of the

(5.13)

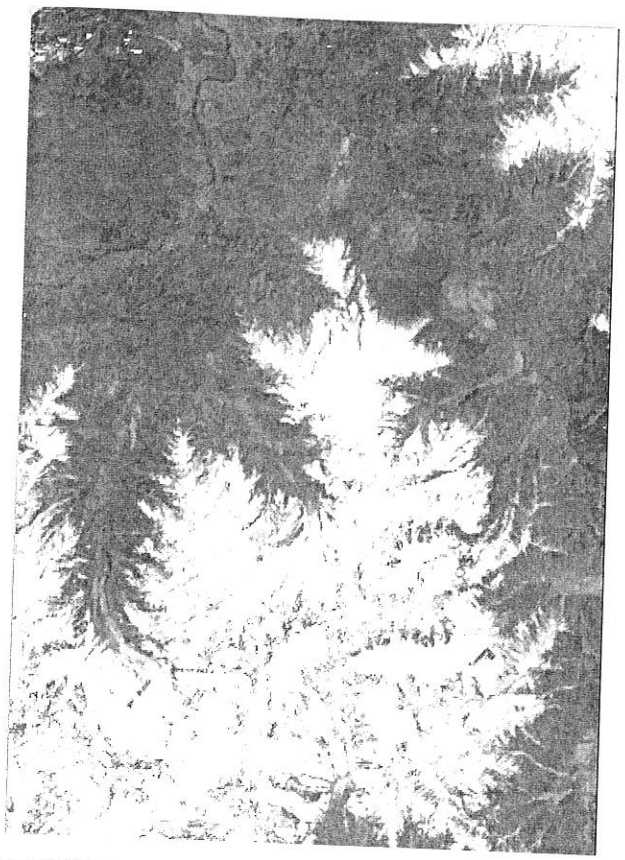

Figure 5.6. *SPOT-3* HRV NIR image of Nanga Parbat after topographic normalization using the Minnaert correction method and multiple k values. These values were computed on the basis of land-cover stratification. Spectral variance is dramatically reduced compared with the original NIR image, although overcorrection occurred at the base of steep slopes (light grey tones). The image size is $\sim 30 \times 40$ km, and north is toward the top of the page.

software development is required to determine what level of simplification is needed to generate reasonable ARC results. Furthermore, field research is required to characterize the nature of the BRDF for alpine land-cover classes.

5.5 GEOMETRIC CALIBRATION

It is especially important to reduce the spatial distortions that are inherent in satellite imagery as a result of sensor geometry, orbital geometry, and the topography of the Earth. Much progress has been made in geometric calibration, which is primarily concerned with repositioning pixel locations in the image array to a known reference grid. In general, geometric correction involves three steps which involve:

- Selection of a suitable mathematical distortion model. This is usually some type of polynomial function.
- Coordinate transformation. Pixel locations are altered by image rotation, and pixel array coordinates are transformed to a coordinate system.
- Spatial interpolation. Interpolated pixel values are generated because of image rotation. Standard interpolation algorithms include nearest neighbor, bilinear, and cubic convolution.

Numerous terms are frequently used to refer to geometric corrections, although these terms have specific meanings. For example, *rectification* refers to the alignment of an image to a planimetric map, while *registration* refers to the alignment of an image to another image, so that two pixels in the same location refer to one location on the Earth surface. Registration and rectification are important for comparing multitemporal data and verifying information extraction results, as land cover classifications and estimates of surface biophysical properties must often be compared with reference data collected in the field.

For mountain applications it is important to note that topography can introduce significant spatial distortions in the imagery, and orthorectification is required so that topographic distortion is removed on a pixel by pixel basis (Bishop et al., 1998b). Orthorectification requires the use of a DEM so that each pixel location can be corrected for relief displacement. The procedure requires the selection of ground control points (GCPs) to constrain the polynomial coefficients.

The objective is to identify pixels that are associated with static objects that do not change over time. These pixels must have corresponding GCPs so that pixel coordinates can be transformed to planimetric coordinates. Image sampling and the collection of GCPs should account for geographic and topographic variability. Orthorectification can be difficult in mountain environments as large-scale topographic maps and/or DEMs are not always available. Similarly, identifying quality control points is problematic due to the dynamic nature of mountain environments. For example, in the western Himalaya, monsoon precipitation, glaciation, frequent mass movements, and catastrophic flooding rapidly alter the land cover and topographic characteristics over various timescales, making it difficult to identify static features. As a result, obtaining a reliable, large sample size can be difficult. The best features are houses, road intersections, and abrupt directional changes in highly reflective trails. With the advent of global positioning system (GPS) technology and GPS receivers, GCPs can be easily collected in the field for planimetric control (e.g., Kardoulas et al., 1996; Gao, 2001).

5.6 REMOTE-SENSING APPLICATIONS

We have a limited understanding of the processes and interactions that govern the complexity of mountain environments (Molnar and England, 1990; Beniston, 1994; Shroder and Bishop, 1998). Major issues include atmosphere–landscape interactions and climate change (Barry, 1994), estimating rates of surface process (Harbor and

ic normalization using
vere computed on the
ed compared with the
teep slopes (light grey
he page.

plification is needed
is required to char-

inherent in satellite
topography of the
which is primarily
a known reference
involve:

Warburton, 1992; Howard, 1996), topographic evolution and relief production (Burbank et al., 1996; Brozovik et al., 1997; Small, 1999; Whipple et al., 1999; Bishop et al., 2002), ecological change (Halpin, 1994; Körner, 1994; Tappeiner et al., 2001), landscape stability and alpine hazards (Shroder, 1989; Bebi et al., 2001), and surface hydrology and water resources (Reinking, 1995; Colby, 2001). Research on these topics is beginning to provide insights on the operational scale of processes and feedback mechanisms, although special emphasis has been focused on external forcing factors.

Only recently have scientists begun to use geographic information science (GIScience) principles and concepts to study the scale-dependent nature of mountain systems (Price and Heywood, 1994; Bishop et al., 1998b). New concepts, data sources, and techniques have provided Earth scientists with new ways to investigate complex problems. In general, remote-sensing research is being used to study mountain environments in the following ways:

- Determination of the optical and thermal properties of the atmosphere, minerals, rocks, soil, vegetation, water, ice, and snow. The capabilities of biophysical remote sensing include the estimation of surface parameters, such as reflectance (Hall et al., 1988; Yang and Vidal, 1990; Chavez, 1996), albedo (Eliason et al., 1981; Robinove et al., 1981; Duguay and LeDrew, 1992), temperature (Wan and Dozier, 1989; Li and Becker, 1993; Lipton and Ward, 1997), topography (Welch et al., 1998), soil properties (Palacios-Orueta and Ustin, 1998; Palacios-Orueta et al., 1999), and forest canopy characteristics (Baret, 1995).
- Landscape mapping. The spatial, spectral, and temporal dimensions associated with remotely sensed data and other spatial data enable geomorphological mapping (Bishop et al., 1998a; Dikau, 1989), mineral and lithologic mapping (Farrand, 1997), vegetation mapping (Ekstrand, 1996; Bochenek et al., 1997), and snow and ice mapping (Haefner et al., 1997; Tappeiner et al., 2001; Williams et al., 1991). Various change detection approaches can be used to determine the magnitude of change which can provide insight into the sensitivity of various features and system dynamics to outside forcing factors.
- Spatial modeling. The integration of remotely sensed data with spatial data in a GIS database can be used to model environmental conditions. Examples include radiation potential (Dozier et al., 1981; Bernhard and Weibel, 1999), hazard potential (Walsh et al., 1990; van Westen 1994), erosion potential (Bishop and Shroder, 2000; Finlayson and Montgomery, 2003), snow cover duration (Tappeiner et al., 2001), and analysis of the topography (Burbank et al., 1996; Brozovik et al., 1997).
- Satellite-derived input parameters and spatial constraints for empirical, deterministic, and stochastic modeling. Biophysical estimates of surface properties and characteristics are required for a variety of modeling efforts. Examples include land cover, area estimates, albedo, radiation potential, topography, and temperature, for regional and global climate modeling (Lee et al., 1993; Skelly et al., 1993), glacier ablation and denudation modeling (Hall et al., 1988; Bishop et al.,

1995), simulations of topographic evolution (Koons, 1995), and models of basin runoff and discharge (Gao et al., 1993; Colby, 2001).

5.6.1 Alpine glaciation

High-latitude and mountain environments are known for their complexity and sensitivity to climate change (Beniston, 1994; Mysak et al., 1996; Meier and Dyurgerov, 2002). In addition to the continental ice masses, several mountain regions have been identified as "critical regions" and include Alaska, Patagonia, and the Himalaya (Haeberli, 1998; Meier and Dyurgerov, 2002). Although smaller in extent, alpine glaciers are thought to be very sensitive to climate forcing due to the altitude range and/or variability in debris cover (Nakawo et al., 1997). Furthermore, such high-altitude geodynamic systems are considered to be the direct result of climate forcing (Molnar and England, 1990; Bishop et al., 2002), although climatic versus tectonic causation is still being debated (e.g., Raymo et al., 1988; Raymo and Ruddiman, 1992). Central to various geological and glaciological arguments is obtaining a fundamental understanding of the feedbacks between climate forcing and glacier response (Hallet et al., 1996; Dyurgerov and Meier, 2000). This requires detailed information about glacier distribution and ice volumes, annual mass balances, regional mass-balance trends, and landscape factors that control ablation. From a practical point of view, the extremely rapidly changing glaciological, geomorphological, and hydrological conditions in the cryosphere present to many regions of the world a "looming crisis" in terms of a decreasing water supply, increased hazard potential, and in some instances geopolitical destabilization.

McClung and Armstrong (1993) have indicated that detailed studies of a few well-monitored glaciers do not permit characterization of regional mass balance trends, the advance/retreat behavior of glaciers, or global extrapolation. Given our current rate of collecting glacier information, it is expected that far too many glaciers will be entirely gone before we can measure and understand them. This time-sensitive issue requires us to acquire global and regional coverage of glaciers via satellite imagery before they disappear. As time is of the essence, a certain level of automation is required, although numerous challenges remain regarding image-based information extraction and validation. Consequently, an integrated approach to studying the cryosphere must be accomplished using remote sensing and GIS investigations to improve our understanding of climate forcing and glacier fluctuations (Haeberli et al., 1998).

Remote sensing of glaciers is increasingly being utilized for scientific studies, as the improved spatial, spectral, and radiometric resolutions of sensors and GIT permit assessment of a variety of glaciological parameters. Satellite imagery provides important spatio-temporal information regarding the distribution of primary types of matter and the characteristics of alpine glaciers. Specifically, information about glacial extent, debris loads, ablation, ice velocity, and transient snowline can be assessed. Quantitative and thematic information can be used for inventory, change detection, and process-based studies. For example, Aniya et al. (1996) did an inventory of outlet glaciers of the southern Patagonia Icefield. They

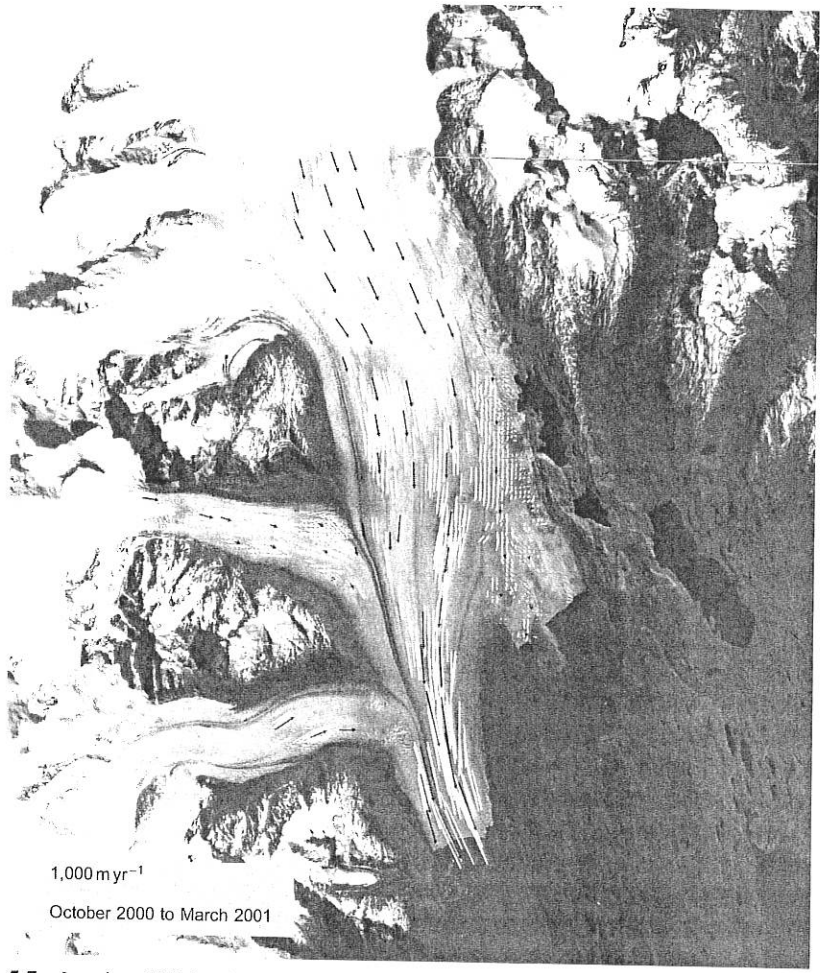

Figure 5.7. *Landsat* ETM+ image acquired 14 October 2001 showing Upsala Glacier, South Patagonia. All velocity vectors obtained from cross correlation-based feature tracking between October 2000 to March 2001 are overlaid as white line segments, and a subset of these are overlaid as black arrows for clarity. Ice surface speed ranges up to just under 2,000 m yr^{-1}. The fast-moving calving front is approximately 2 km wide.

From Skvarca et al. (2003).

extracted 11 parameters related to glacier morphology and they indicated that the methods used produced results comparable with results generated from topographic maps. In addition, quantitative assessment of physical characteristics, such as ice velocity vectors, permit better understandings of glacier-related processes including mass balance, ice deformation, and erosion (Figure 5.7).

Research continues to evaluate data from sensor systems and the evaluation of information extraction techniques/approaches. These studies include alpine snow mapping (Dozier and Marks, 1987; Haefner et al., 1997), assessing and mapping

Upsala Glacier, South
ısed feature tracking
ients, and a subset of
ges up to just under
e.

y indicated that the
d from topographic
eristics, such as ice
processes including

d the evaluation of
ıclude alpine snow
ssing and mapping

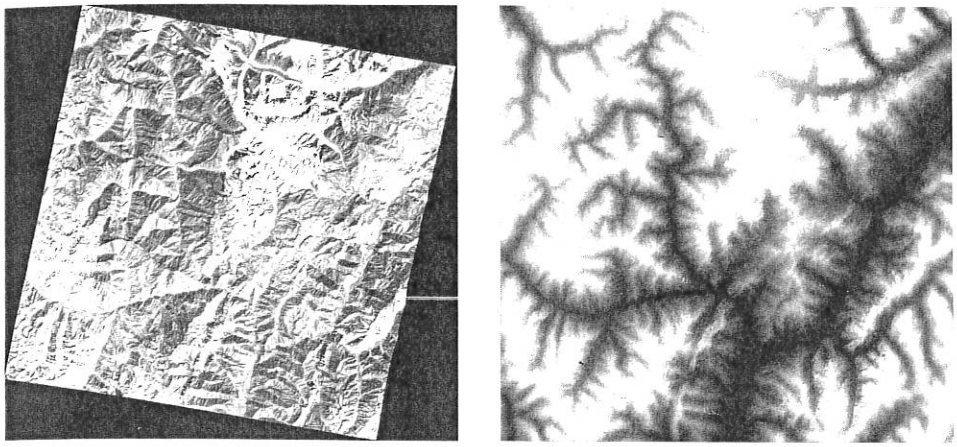

Figure 5.8. DEM generated using ASTER data in complex topography. This ASTER false-color composite (grayscale depiction) of the Hindu Kush in northwestern Pakistan and Afghanistan depicts the rugged terrain (left). The DEM (right) depicts high-frequency topography variation that is needed for geomorphometry, ARC, and glacier mapping. The scene is $\sim 60 \times 60$ km.

supraglacial features (Bishop et al., 1995, 1998a, 1999), and mapping of glacier ice and snow facies (Hall et al., 1988; Williams et al., 1991). This work has been frequently concerned with accurate delineation of glaciers and comparison of satellite-derived surface reflectance with *in situ* measurements. Results from these and other studies have indicated that high-resolution spectral data and topographic information are required for assessing present day glacierization and past glaciation (Hall et al., 1989; Brozovik et al., 1997; Bishop et al., 2001).

Satellite-derived topographic information is critical for geomorphological and glaciological studies. For example, the ASTER sensor aboard *Terra* provides DEM generation capabilities for full scenes (60×60 km). Standardized photogrammetric procedures can be used to produce reasonably high-quality DEMs over large areas. However, numerous DEM generation methodological problems exist (Figure 5.8). DEMs are required for geomorphometric analysis and characterization of the terrain, orthorectification of satellite imagery to remove spatial and relief distortion, ARC to remove atmospheric and topographic effects, numerical modeling of surface processes, and glacier morphometric mapping.

Multispectral analysis of debris-covered glaciers, which are characteristic of many regions of the world, still represents a significant remote-sensing problem that has not been thoroughly investigated (Bishop et al., 1995, 1998a, 1999, 2001). Similarly, there is a paucity of quantitative, remote-sensing studies designed to examine and characterize supraglacial characteristics. Consequently, a comprehensive approach to information extraction and glaciological characterization of glaciers from space is sorely needed.

Bishop et al. (2001) discussed the importance of characterizing the hierarchical nature of mountain topography as it relates to surface processes and glacier

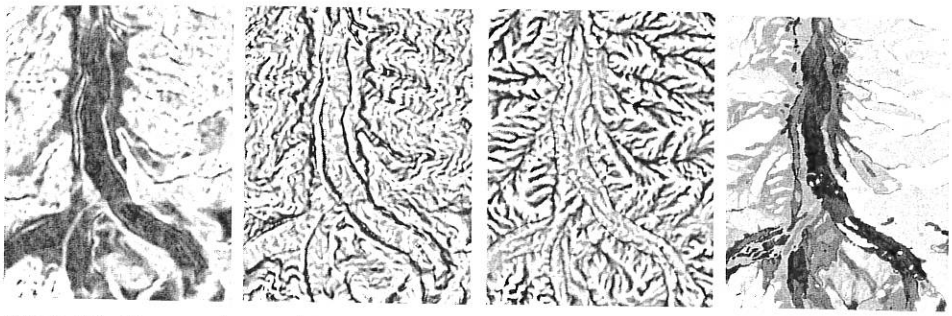

Figure 5.9. Geomorphometric parameters and object-oriented glacier mapping for the Raikot Glacier at Nanga Parbat. The images from left to right are: (1) slope angle map; (2) profile curvature map; (3) tangential curvature map; (4) automated, glacier delineation map. Geomorphometric parameters can be used to delineate debris-covered glaciers, and the mapping model does a good job in identifying and delineating the majority of the ablation zone. Problem segments of the glacier can be addressed using advanced 3-D spatial analysis. The scene is $\sim 6 \times 8$ km.

mapping. They also demonstrated the ability to recognize and characterize process-form relationships and were able to accurately delineate and map alpine glaciers using a satellite-derived DEM. The hierarchical modeling of topography is an important step in understanding topographic forcing on surface processes and in identifying the operational scale of glaciation on the landscape (Bishop et al., 2001). They used geomorphometric analysis and object-oriented spatial analysis to generate morphometric and, potentially, morphogenetic information. The mapping model worked very well for complex debris-covered glaciers in the Himalaya (Figure 5.9).

Assessing and mapping glaciers from space using traditional approaches will permit the production of baseline information that allows change detection studies. The use of various techniques and brute-force classification algorithms, however, do not produce consistently high-quality results (Bishop et al., 1999), and production of quality information commonly requires significant pre-analysis steps and *a priori* knowledge of the study area. Consequently, new technologies and approaches must be pursued, although results must be validated by data collected in the field.

Diagnostic capabilities should become feasible when detailed spectral and spatial information are integrated into physical models that characterize process-form relationships. Topographic evolution, climate, solar radiation transfer, and surface energy-budget simulations which make use of DEMs, satellite imagery, and satellite-derived thematic and biophysical information should provide additional insights into glacier processes, climate change, and the geodynamics of mountain building. Integrative research involving GIScience, geomorphology, and glaciology is required to permit assessment of alpine landscapes using geomorphological, material/properties, and surface process information. Such a systematic approach to characterizing glaciers from space will permit regional mass-balance trends to be more reliably determined, so that global analyses and understandings of the Earth's

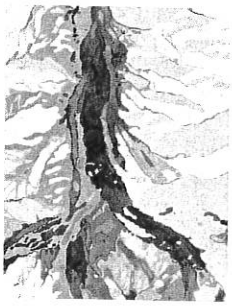

lapping for the Raikot
angle map; (2) profile
lelineation map. Geo-
iers, and the mapping
of the ablation zone.
) spatial analysis. The

haracterize process-
map alpine glaciers
topography is an
ce processes and in
Bishop et al., 2001).
analysis to generate
he mapping model
alaya (Figure 5.9).
al approaches will
change detection
ication algorithms,
shop et al., 1999),
ificant pre-analysis
w technologies and
by data collected in

spectral and spatial
process-form rela-
nsfer, and surface
llite imagery, and
provide additional
amics of mountain
gy, and glaciology
geomorphological,
stematic approach
alance trends to be
lings of the Earth's

icemass fluctuations will be based on high-quality information, not just static spatial snapshots through time.

5.6.2 Landscape ecology

The use of remote sensing in landscape ecology is becoming ever-more extensive (e.g., Greegor, 1986; Hall et al., 1988; Nellis and Briggs, 1989; Turner and Gardner, 1991; Metzger and Muller, 1996), although there is a paucity of remote-sensing research in mountain ecosystems using thermal infrared (TIR) remote-sensing data for the study of landscape processes. The primary use of TIR data in mountainous regions has been for mapping of geologic formations (Hook et al., 1992; Crowley and Hook, 1996; Schmugge et al., 1998). Despite the difficulties of working in mountain environments, the potential is high for use of TIR remote-sensing data to provide important new information in the analysis and modeling of landscape ecological phenomena (Graetz, 1990; Luvall and Holbo, 1991; Quattrochi and Pelletier, 1991; Norman et al., 1995).

TIR remote-sensing data are particularly useful for understanding the fluxes and redistribution of materials among landscape elements (Risser et al., 1984). Thus, the observation, measurement, and analysis of thermal fluxes, as they contribute to energy balance characteristics, is an implicit and important aspect of landscape dynamics and landscape functioning in mountain terrain.

We provide examples of both airborne and spaceborne TIR data in studying the landscape characteristics in mountainous areas. Moreover, NASA's EOS *Terra* satellite platform offers a number of new remote-sensing systems that have improved spatial resolutions and better calibrated TIR data (see Table 5.1).

Airborne thermal remote sensing

Much of the initial and ongoing research in thermal remote sensing in mountain terrain was done using airborne instruments. Airborne sensors are typically configured to closely match the spectral characteristics of either current or planned future satellite systems. They provide valuable research data sets for the development of algorithms for radiometric calibration and image analysis of satellite data. Many of these instruments are similar to the Advanced Thermal and Land Applications Sensor (ATLAS). ATLAS is a 15-channel airborne sensor that incorporates the bandwidth range of TM, with additional bands in the mid-reflective infrared and TIR range. ATLAS can collect multiresolution (2–25 m) data. All of the channels have onboard calibration, which permits verification of radiometry on an ongoing basis. Visible channel calibration is provided by an onboard integrating sphere. Calibration of the thermal channel is provided by onboard blackbodies.

The ATLAS sensor is particularly attractive for data collection in mountain areas for several reasons. All bands share the same spatial resolution. This permits direct comparison of radiometry across all channels. In addition, the sensor has superior spectral resolution within the TIR channels. These offer the potential to

make accurate measurements of thermal responses for different landscape characteristics and their corresponding land–atmosphere interactions over small wavelength regions. The data from an onboard GPS system can be combined with DEMs through an automated georectification process to account for terrain effects.

TIR atmospheric correction and calibration

As discussed in Section 5.4 the atmosphere has considerable impact on the amount of thermal radiation emitted from the Earth's surface and that measured by an airborne or satellite remote-sensing system. As TIR radiation passes through the atmosphere, it is attenuated by the processes of scattering and absorption. In the TIR portion of the electromagnetic spectrum, absorption of radiation by gas molecules is of more significance than is scattering. Strong absorption by water vapor and carbon dioxide molecules restricts atmospheric transmission of TIR radiation to two "windows", one at 3–5 μm and a larger one at 8–14 μm. The 8–14 μm region of the spectrum is of particular interest in TIR remote sensing because it contains the peak energy emissions for most Earth surface features (i.e., at approximately 9.7 μm). Thus most thermal remote sensing is performed within this region of the electromagnetic spectrum.

Although TIR remote sensing utilizes the two atmospheric windows noted above, the intervening atmosphere between the Earth's surface and the sensor alters spectral response and, if left uncorrected, may bias estimates of surface temperature. Gases and suspended particles in the atmosphere absorb radiation emitted by targets on the ground, and this radiation is re-emitted back into the atmosphere.

The measurement and modeling of the atmospheric correction needed to produce calibrated data sets from ATLAS are extremely complex procedures. They require direct measurements of the atmospheric extinction coefficients that are a function of wavelength. Calibration of the ATLAS instrument is also required. MODTRAN4 was used to model the atmospheric radiance and transmittance using input from radiosonde data and shadow band radiometers (Berk et al., 1999).

Surface energy budget

Surface temperature is a major component of the surface energy budget. Knowledge of it is important in any attempt to describe the radiative and mass fluxes that occur at the surface. Use of energy terms in modeling surface energy budgets allows the direct comparison of various land surfaces encountered in a landscape, from vegetated (forest and herbaceous) to nonvegetated (bare soil, roads, and buildings) (Oke, 1987). The partitioning of energy-budget terms depends on the surface type. In natural landscapes the partitioning is dependent on canopy biomass, leaf area index, aerodynamic roughness, and moisture status, all of which are influenced by the development stage of the ecosystem.

The net all-wave, radiation balance ($W\,m^{-2}$) of landscape canopies can be determined following Oke (1987). Net solar radiation (K^*), is given by:

$$K^* = (1.0 - \alpha)K^{\downarrow} \tag{5.14}$$

where α is the hemispherical albedo that represents the ratio of the radiant flux to the irradiance, and $K^{\downarrow}$ is the irradiance.

The long-wave energy emitted from a surface ($L^{\uparrow}$) is dependent on surface temperature such that:

$$L^{\uparrow} = \varepsilon[\sigma T^4] \tag{5.15}$$

where ε is the emissivity, σ is the Stefan-Boltzmann constant ($5.7 \times 10^{-8}\,W\,m^{-1}\,K^{-4}$), and T is the land surface temperature (K).

The net long-wave radiation at the surface (L^*) is given by:

$$L^* = L^{\downarrow} - L^{\uparrow} \tag{5.16}$$

where $L^{\downarrow}$ is long-wave radiation from the atmosphere. Therefore, the net all-wave radiation (R_n) can be given as:

$$R_n = K^* + L^* \tag{5.17}$$

Net radiation is a particularly useful term because, under most conditions, it represents the total amount of energy available to the land surface for partitioning into nonradiative processes (mass heating, biological synthesis, etc.) at the surface. It is the amount of energy the system holds on to and degrades. In vegetated areas the amount of net radiation is dependent on vegetation type and varies with canopy leaf area and structure.

Net radiation may be expressed as the sum of these nonradiative fluxes:

$$R_n = \lambda E + H + G \tag{5.18}$$

where H is the sensible heat flux, λ is the latent heat of vaporization of water, E is the transpiration flux, and G is the energy flux into or out of storage (both canopy and soil).

The partitioning of λE, H, and G is also dependent on the make-up of the surface. Both the physiological control of moisture loss (stomatal resistance) and leaf/canopy morphology for vegetation determines how R_n is partitioned among λE, H, and G.

The Penman–Monteith equation (Monteith, 1973) can be used to illustrate these factors. It combines those environmental factors and plant factors that are important in determining λE:

$$\lambda E = \frac{s(R_n - G) + \left[\dfrac{\rho_a C_p D}{R_a}\right]}{s + \gamma\left[1.0 + \dfrac{R_c}{R_a}\right]} \tag{5.19}$$

where s is the slope of the saturation vapor–pressure relationship, ρ_a is the density of air, C_p is the specific heat of air, D is the vapor-density deficit of the air, γ is the

psychrometric constant, R_a is aerodynamic resistance, and R_c is canopy resistance (stomatal resistance/leaf area index). To solve for surface temperature T_s:

$$T_s = T_a + \frac{R_b}{C_p}(R_n - \lambda E) \tag{5.20}$$

where T_a is air temperature, and R_b is boundary layer (aerodynamic) resistance. The remotely sensed data obtained from the ATLAS sensor allows the measurement of important terms in radiative surface energy budget: $K^{\uparrow}$ (reflected solar radiation) and $L^{\uparrow}$ on a landscape scale in mountain terrain. When combined with output from MODTRAN4 atmospheric-radiance models, the remaining terms $K^{\downarrow}$ and R_n can be determined (Berk et al., 1999).

Forest canopy temperature

The spatial variation of canopy temperatures across the landscape depicts a complex pattern. Differential illumination due to topography can produce significant spatial variation of canopy temperatures, even in single-species canopies of uniform age and structure. The variability in illumination and differences in surface albedo are illustrated in Figure 5.10 (see color plates) using an image derived from 10 m ATLAS data flown over Salt Lake City and the Wasatch Mountains. The resulting surface temperatures in the thermal map of the same area (Figure 5.11, see color plates) are dependent on the illumination, vegetation type and cover, and geologic material.

Thermal remote sensing is useful for assessing the spatial variability of forest canopy temperature for choosing sites for instrument placement. Forest canopy temperatures that exhibit a bimodal frequency distribution contain two populations of canopy temperatures with two different surface energy budgets and would require two sets of tower-based instruments to sample the canopy.

A good example of the effect of topography on surface energy budgets is given in Table 5.2. The latent heat flux values estimated from the Thermal Infrared Multispectral Scanner (TIMS) and Penman–Monteith values determined from tower-measured fluxes were similar during the mid-day flights. For the morning

Table 5.2. Latent heat fluxes ($W\,m^{-2}$) from a white pine canopy at the U.S. Forest Service's Coweeta Hydrologic Laboratory, NC, determined from remotely sensed surface temperatures (Thermal Infrared Multipectral Scanner), needle thermocouple temperatures, and surface energy budgets.

Time ending	08 : 25	08 : 55	13 : 00	13 : 25
Penman–Monteith	76	92	467	504
TIMS data	460	296	449	385
Range*	225–601	157–436	325–600	282–489

* The lowest and highest individual pixel temperatures were used for evapotranspiration estimates for the time period.

Modified from Luvall (1997).

period, however, the TIMS values were considerably greater than either the Penman–Monteith or the thermocouple values. Several factors may account for these differences. For the morning period the canopy temperatures varied spatially across the canopy around the tower, with the lowest canopy temperatures directly around the tower. The average latent heat flux ($n = 1{,}000$) was determined from 5-m pixels surrounding the tower that included nonshaded and much warmer areas of the canopy. If we examine the latent heat flux calculated from the lowest pixel temperatures they are 157–225 $W\,m^{-2}$, which is much closer to the Penman–Monteith value of 76 and 92 $W\,m^{-2}$. Portions of the canopy were wet around the tower, but it is difficult to quantify the partially wet canopy (R_c). If we assume the entire canopy around the tower was wet ($R_c = 0.0$), then the Penman–Monteith values for the time periods 08 : 25 and 08 : 55 become 381 and 528 $W\,m^{-2}$, which are similar to the TIMS estimates.

Beta index and temperature spatial variation

The average temperature for a forest canopy cannot express the spatial variability. Holbo and Luvall (1989) have demonstrated, however, that the frequency distributions of temperatures can be used as a powerful model in differentiation and identification of the cover types and properties of the land surface. They found that a beta probability distribution most closely resembles the observed temperature frequency distributions from forested landscapes. An advantage of using the beta distribution as a model is that it utilizes pixel frequency distributions directly and no higher order statistics that magnify measurement error are used. They developed a beta index by which these forested landscapes could be classified.

The beta index measures the spatial variability of temperature within an ecosystem. As ecosystems develop, nonequilibrium thermodynamic theory suggests that they would tend toward internal equilibrium. Therefore, we would expect the spatial variability of temperature to decrease as an ecosystem develops. Thus a large beta index should indicate a more developed ecosystem. An example from Holbo and Luvall (1989) is given in Table 5.3. The observed surface temperature frequency distribution curves for the five sites were used to develop a beta index. The frequency distributions were characteristic of each surface. By examining each frequency distribution it is apparent that pixels with vegetation are much cooler than those with bare soil and a mixture of canopy and soil. Sites with a more developed canopy had a much narrower and uniform temperature distribution. The beta index ranged from a low of −12.9 for the quarry site to a high of 130.1 for the old-growth Douglas fir forest site (Table 5.3). The lower beta index value represented surfaces that had little or no vegetation cover. As the forest canopy became more uniform and developed the beta index increased.

The change in surface temperature as a function of time is an additional property that can be measured using thermal remotely sensed data. This may be done using repeated overflights. Usually, a separation of about 30 minutes results in a measurable change in surface temperature caused by the change in incoming solar

Table 5.3. Radiative transfer estimates, surface temperatures derived from thermal remote-sensing measurements, beta index, and TRN values (equation 5.21) for several surface types at the Andrews Experimental Forest in Oregon. Site identification designators are QUARRY for quarry, CLRCUT for clearcut; NATREG for natural regeneration, PLANT for plantation, and MATUREF for old-growth Douglas fir forest.

	QUARRY	CLRCUT	NUTREG	PLANT	MATUREF
K^* ($W\,m^{-2}$)	718	799	895	854	924
Albedo	0.25	0.22	0.15	0.15	0.8
L^* ($W\,m^{-2}$)	273	281	124	124	92
R_n ($W\,m^{-2}$)	445	517	771	730	832
R_n/K^* (%)	62	65	86	85	90
T (°C)	50.7	51.8	29.4	29.5	24.3
ΔT (°C)	4.5	2.2	1.7	0.8	0.7
Beta parameter α, β	41, 8	20, 4	55, 95	120, 200	210, 520
Beta index	−12.9	−6.3	17.2	34.4	130.1
TRN ($kJ\,m^{-2}\,°C^{-1}$)	168	406	788	1,631	2063

Modified from Holbo and Luvall (1989) and Luvall and Holbo (1989).

radiation. Their ratio can be used to define the surface property that Luvall and Holbo (1989) called a Thermal Response Number (TRN), such that:

$$TRN = \frac{\int_{t_1}^{t_2} R_n\, dt}{\Delta T} \tag{5.21}$$

where R_n is total net radiation and ΔT is the change in surface temperature for time period t_1 to t_2.

The TRN provides an analytical framework for studying the effects of surface thermal response for large spatial resolution map scales that can be aggregated for input to smaller scales, as needed by climate models. The importance of TRN is that: (1) it is a functional classifier of land cover types; (2) it provides an initial surface characterization for input to various climate models; (3) it is a physically based measurement; (4) it can be determined completely from remotely sensed data; and (5) it is a scale-independent measurement that can be examined from a pixel by pixel measurement or for a polygon from a landscape feature which represents a group of pixels. The TRN can be used as an aggregate expression of both surface properties (forest canopy structure and biomass, age, and physiological condition; urban structures and material types) and environmental energy fluxes.

The TRN has been used previously in Douglas fir forests in the Pacific Northwest to assess differences in canopy structure/biomass due to stand age (Luvall and Holbo, 1989). Large differences were found among the forest types, where the TRN ranged from 406 $kJ\,m^{-2}\,°C^{-1}$ for a 2-year-old replanted clearcut to 2,063 $kJ\,m^{-2}\,°C^{-1}$ for a 400-year-old Douglas fir forest. The surfaces containing mostly soil and bare rock exhibited the lowest TRN, whereas forested surfaces

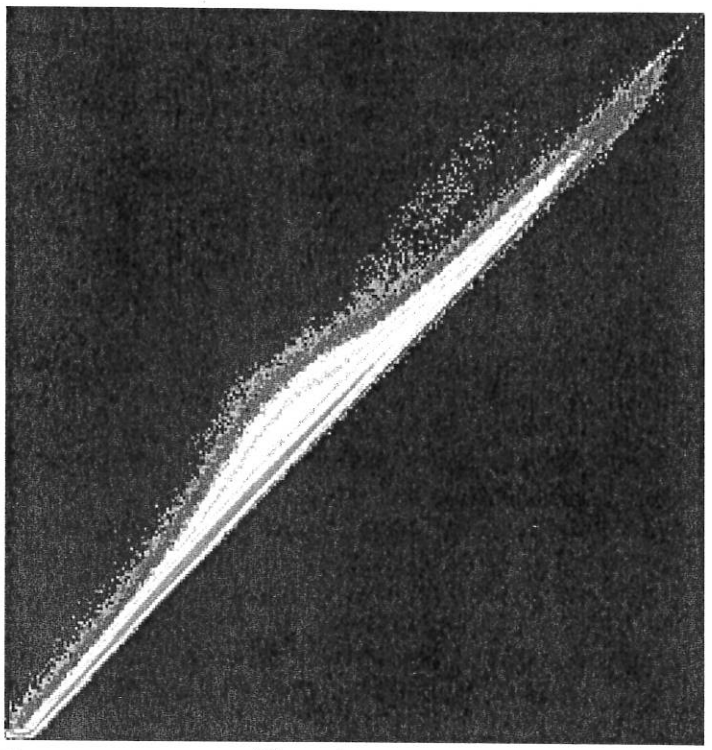

Figure 5.12. Scatterplot of ATLAS thermal channels 13 and 12 which shows emissivity variation with wavelength. Emissivity differences for Salt Lake City flight 5.71.

exhibited the highest values. Results indicate that the TRN derived from average surface temperatures and radiation balance estimates is a site-specific surface property that can discriminate among various types of coniferous forest stands.

Most of the early work in mountain terrain using thermal data is based on the use of multispectral thermal data collected from aircraft to map geological formations (Kahle et al., 1980; Hook et al., 1992). The use of multispectral thermal data is critical because some geological materials do not exhibit a uniform emissivity across the thermal spectrum. The effect of emissivity changes of the surface can be illustrated by plotting two ATLAS thermal channels, 12 and 13, from a single flightline over the eastern edge of Salt Lake City and the Wasatch Mountains (Figure 5.12). A constellation of points that plot along a 45° slope indicate little or no deviation from an emissivity of 1. Departure from the line defined by spectral grey materials must be caused by variation in emissivity between channels. Sensor noise causes dispersion from an ideal line. These emissivity differences, caused by different geological formations, are dramatic, as shown in a false color composite image (ASTER thermal

infrared bands 13, 12, and 10) from the Saline Valley area of California (Figure 5.13, see color plates).

5.7 FUTURE RESEARCH DIRECTIONS

Given the non-Lambertian nature of snow, ice, forest canopies, and other surfaces (Dozier, 1980; Hall et al., 1989; Gu and Gillespie, 1998; Greuell and de Ruyter de Wildt, 1999), more research is required to characterize the BRDF of alpine landscapes. The problem is complex, as solar geometry and scale-dependent topographic effects control irradiant and radiant flux. In addition, the topography affects other factors, such as moisture, surface stability, snow accumulation, forest canopy structure, and other land-surface parameters that affect the BRDF and thermal radiant flux. Therefore, more research is required to understand and model the scale-dependent nature of radiation transfer in mountains. New understandings will have an impact on other environmental models that must include radiative transfer processes and include surface-parameter estimates generated from satellite imagery.

Toward this goal, Earth scientists have developed empirical, semi-empirical, and deterministic models that attempt to address the problem of anisotropic reflectance. Research has demonstrated that empirical and semi-empirical approaches are often scene-dependent and will not work over a wide range of topographic and land cover conditions. On the other hand, deterministic models have a physical basis, but frequently require *in situ* measurements at the time of image acquisition. Their use can be problematic given the limited amount of information on atmospheric and land surface conditions.

We suggest that the solution to the problem is the development of new ARC models that have a physical basis and account for the influence of the atmosphere, topography, and land cover. A solution dictates finding an acceptable level of simplification, such that reliable estimates of irradiant and radiant fluxes can be generated by incorporating satellite imagery and DEMs into physical radiation transfer models.

For various mountain applications, satellite data have been relied on for mapping and monitoring. The relationship between spectral response and surface processes, however, is notoriously complex. Consequently, per pixel analysis and traditional statistical procedures for pattern recognition do not adequately enable landform mapping (McDermid and Franklin, 1995). Even forest mapping can be difficult, and numerous investigators have developed new algorithms to account for high spectral variability (e.g., Franklin and Wilson, 1992).

These limitations have been sought to be overcome by the integration of DEMs into models and analysis procedures (Franklin and Wilson, 1992; McDermid and Franklin, 1995; Pike and Park, 1995). Progress in this direction has been limited

because of the issue of scale as it relates to data, spatial analysis, and characterizing the operational scale over which surface processes and feedback mechanisms operate (Quattrochi and Goodchild, 1997; Bishop et al., 1998a). Therefore, new techniques and modeling approaches are required to address geoscience problems (Small, 1999).

Quattrochi and Goodchild (1997) and Tate and Atkinson (2001) addressed the problem of scale and provided examples of concepts, geostatistical techniques, and modeling approaches that can help Earth scientists analyze spatial data. More research regarding spatial information extraction from satellite imagery and DEMs is a starting point. Traditional approaches that rely on arbitrarily sized ground segments (i.e., window size) for calculation of image or terrain texture, or other first- and second-order topographic parameters, do not address the issue of scale-dependent features and processes (McDermid and Franklin, 1995; Pike and Park, 1995). Numerous investigations have indicated that more advanced types of spatial analysis and modeling will be required to address this most difficult problem (Davis et al., 1991; McDermid and Franklin, 1995). For example, McDermid and Franklin (1995) used semivariogram analysis to determine the scale at which to compute geomorphometric parameters. Bishop et al. (1998a) found that semivariogram analysis of imagery could be used for supraglacial geomorphological mapping, although landform-scale problems limited the approach.

Alpine landscapes are spatially complex, and contextual information extraction is also required. Contextual information includes direction, distance, connectivity, and other topological relationships. New developments that include object-oriented modeling and analysis, and 3-D GISs will enable scientists to explore the applicability of fuzzy theory and hierarchy theory, and begin to characterize and model spatial constraints and the complex organization of mountain landscapes. New spatial algorithms and 3-D spatial-modeling capabilities will enable better contextual characterization. This will enable advanced spatial modeling and analysis of the landscape based on physical principles.

More research into object-oriented analysis and modeling is warranted. Numerous investigators have indicated that the hierarchical organization of mountain topography can be modeled using hierarchy theory and object-oriented modeling (Dikau, 1989; Raper and Livingstone, 1995). Utilization of satellite imagery and DEMs for landform classification is therefore possible, and modeling efforts may provide new insights into process-form relationships and system dynamics. Furthermore, this approach is well suited for integrating land cover objects produced from classification of remotely sensed data.

Ultimately, environmental models must incorporate spatial concepts, new data models, and spatial data to simulate the system dynamics in mountain environments. This will require the coupling of distinct environmental models so that complex feedback mechanisms involving climate, tectonic and surface processes can be studied. Remote-sensing science and GITs play important roles, as they can facilitate the study of the spatial and temporal dimensions of mountain systems.

REFERENCES

Allen, T. R. (1998). Topographic context of glaciers and perennial snowfields, Glacier National Park, Montana. *Geomorphology*, **21**:207–216.

Aniya, M., Sato, H., Naruse, R., Skvarca, P., and Casassa, G. (1996). The use of satellite and airborne imagery to inventory outlet glaciers of the southern Patagonia icefield, South America. *Photogrammetric Engineering and Remote Sensing*, **62**(12):1361–1369.

Baret, F. (1995). Use of spectral reflectance variation to retrieve canopy biophysical characteristics. In: F. M. Danson and S. E. Plummer (eds), *Advances in Environmental Remote Sensing* (pp. 33–51). John Wiley & Sons, Chichester, UK.

Barry, R. G. (1994). Past and potential future changes in mountain environments: A review. In: M. Beniston (ed.), *Mountain Environments in Changing Climates* (pp. 3–33). Routledge, London.

Bebi, P., Kienast, F., and Schnenberger, W. (2001). Assessing structures in mountain forests as a basis for investigating the forests' dynamics and protective function. *Forest Ecology and Management*, **145**:3–14.

Beniston, M. (ed.) (1994). *Mountain Environments in Changing Climates*. Routledge, London.

Beratan, K. K. and Anderson, R. (1998). The use of Landsat Thematic Mapper data for mapping and correlation of Quaternary geomorphic surfaces in the southern Whipple Mountains, California. *International Journal of Remote Sensing*, **12**:2345–2359.

Berk, A., Anderson, G. P., Acharya, P. K., Chetwynd, J. H., Bernstein, L. S., Shettle, E. P., Matthew, M. W., and Adler-Golden, S. M. (1999). *MODTRAN4 Users' Manual*. Air Force Research Laboratory, Hanscom AFB, MA.

Bernhard, L. and Weibel, R. (1999). Modelling snowmelt using a digital terrain model and GIS-based techniques. In: R. Dikau and H. Saurer (eds), *GIS for Earth Surface Systems: Analysis and Modelling of the Natural Environment* (pp. 26–46). Gebrüder Borntraeger-Verlag, Berlin.

Bishop, M. P. and Colby, J. D. (2002). Anisotropic reflectance correction of SPOT-3 HRV imagery. *International Journal of Remote Sensing*, **23**(10):219–222.

Bishop, M. P. and Shroder, Jr, J. F. (2000). Remote sensing and geomorphometric assessment of topographic complexity and erosion dynamics in the Nanga Parbat massif. In: M. A. Khan, P. J. Treloar, M. P. Searle, and M. Q. Jan (eds), *Tectonics of the Nanga Parbat Syntaxis and the Western Himalaya* (Special Publication No. 170, pp. 181–200). Geological Society, London.

Bishop, M. P., Shroder, Jr, J. F., and Ward, J. L. (1995). SPOT multispectral analysis for producing supraglacial debris-load estimates for Batura Glacier, Pakistan. *Geocarto International*, **10**(4):81–90.

Bishop, M. P., Shroder, Jr, J. F., Hickman, B. L., and Copland, L. (1998a). Scale dependent analysis of satellite imagery for characterization of glacier surfaces in the Karakoram Himalaya. *Geomorphology*, **21**:217–232.

Bishop, M. P., Shroder, Jr, J. F., Sloan, V. F., Copland, L., and Colby, J. D. (1998b). Remote sensing and GIS technology for studying lithospheric processes in a mountain environment. *Geocarto International*, **13**(4):75–87.

Bishop, M. P., Shroder, Jr, J. F., and Hickman, B. L. (1999). High resolution satellite imagery and neural networks for information extraction in a complex mountain environment. *Geocarto International*, **14**(2):17–26.

Bishop, M. P., Bonk, R., Kamp, Jr, U., and Shroder, Jr, J. F. (2001). Terrain analysis and data modeling for alpine glacier mapping. *Polar Geography*, **24**(4):257–276.

Bishop, M. P., Shroder, Jr, J. F., Bonk, R., and Olsenholler, J. (2002). Geomorphic change in high mountains: A western Himalayan perspective. *Global and Planetary Change*, **32**:311–329.

Blaszczynski, J. S. (1997). Landform characterization with geographic information systems. *Photogrammetric Engineering and Remote Sensing*, **63**(2):183–191.

Bochenek, Z., Ciolkosz, A., and Iracka, M. (1997). Deterioration of forests in the Sudety Mountains, Poland, detected on satellite images. *Environmental Pollution*, **98**(3):375–379.

Brabyn, L. (1997). Classification of macro landforms using GIS. *ITC Journal*, **1**:26–40.

Brozovik, N., Burbank, D. W., and Meigs, A. J. (1997). Climatic limits on landscape development in the northwestern Himalaya. *Science*, **276**:571–574.

Burbank, D., Leland, J., Fielding, E., Anderson, R. S., Brozovik, N., Reid, M. R., and Duncan, C. (1996). Bedrock incision, rock uplift and threshold hillslopes in the northwestern Himalaya. *Nature*, **379**:505–510.

Chavez, Jr, P. S. (1988). An improved dark-object subtraction technique for atmospheric scattering correction of multispectral data. *Remote Sensing of the Environment*, **24**:459–479.

Chavez, Jr, P. S. (1989). Radiometric calibration of Landsat thematic mapper multispectral images. *Photogrammetric Engineering and Remote Sensing*, **55**(9):1285–1294.

Chavez, Jr, P. S. (1996). Image-based atmospheric corrections—revisited and improved. *Photogrammetric Engineering and Remote Sensing*, **62**(9):1025–1036.

Civco, D. L. (1989). Topographic normalization of Landsat thematic mapper digital imagery. *Photogrammetric Engineering and Remote Sensing*, **55**(9):1303–1309.

Cline, D. W., Bales, R. C., and Dozier, J. (1998). Estimating the spatial distribution of snow in mountain basins using remote sensing and energy balance modeling. *Water Resources Research*, **34**(5):1275–1285.

Colby, J. D. (1991). Topographic normalization in rugged terrain. *Photogrammetric Engineering and Remote Sensing*, **57**(5):531–537.

Colby, J. D. (2001). Simulation of a Costa Rican watershed: Resolution effects and fractals. *Journal of Water Resources Planning and Management*, **127**(4):261–270.

Colby, J. D. and Keating, P. L. (1998). Land cover classification using Landsat TM imagery in the tropical highlands: The influence of anisotropic reflectance. *International Journal of Remote Sensing*, **19**(8):1459–1500.

Conese, C., Gilabert, M. A., Maselli, F., and Bottai, L. (1993a). Topographic normalization of TM scenes through the use of an atmospheric correction method and digital terrain models. *Photogrammetric Engineering and Remote Sensing*, **59**:1745–1753.

Conese, C., Gilabert, M. A., Maselli, F., and Bottai, L. (1993b). Topographic normalization of TM scenes through the use of an atmospheric correction method and digital terrain models. *Photogrammetric Engineering and Remote Sensing*, **59**(12):1745–1753.

Conese, C., Maracchi, G., and Maselli, F. (1993c). Improvement in maximum likelihood classification performance on highly rugged terrain using principal components analysis. *International Journal of Remote Sensing*, **14**(7):1371–1382.

Crowley, J. K. and Hook, S. J. (1996). Mapping playa evaporite minerals and associated sediments in Death Valley, California, with thermal infrared images. *Journal of Geophysical Research*, **101**(B1):643–660.

Danson, F. M., Plummer, S. E., and Briggs, S. A. (1995). Remote sensing and the information extraction problem. In: F. M. Danson and S. E. Plummer (eds), *Advances in Environmental Remote Sensing* (pp. 171–177). John Wiley & Sons, Chichester, UK.

Davis, F. W., Quattrochi, D. A., Kidd, M. K., Lam, N. S. N., Walsh, S. J., Michaelsen, J. C., Franklin, J., Stow, D. A., Johannse, C. J., and Johnston, C. A. (1991). Environmental

analysis using integrated GIS and remotely sensed data: Some research needs and priorities. *Photogrammetric Engineering and Remote Sensing*, **57**(6):689–697.

Dikau, R. (1989). The application of a digital relief model to landform analysis in geomorphology. In: J. Raper (ed.), *Three Dimensional Applications in Geographical Information Systems* (pp. 51–77). Taylor & Francis, London.

Dozier, J. (1980). A clear-sky spectral solar radiation model for snow-covered mountainous terrain. *Water Resources Research*, **16**(4):709–718.

Dozier, J. (1989). Spectral signature of alpine snow cover from the Landsat Thematic Mapper. *Remote Sensing of the Environment*, **28**:9–22.

Dozier, J. and Marks, D. (1987). Snow mapping and classification from Landsat Thematic Mapper data. *Annals of Glaciology*, **9**:97–103.

Dozier, J., Bruno, J., and Downey, P. (1981). A faster solution to the horizon problem. *Computers and Geosciences*, **7**(1):145–151.

Duguay, C. R. and LeDrew, E. F. (1992). Estimating surface reflectance and albedo from Landsat-5 Thematic Mapper over rugged terrain. *Photogrammetric Engineering and Remote Sensing*, **58**(5):551–558.

Dyurgerov, M. B. and Meier, M. F. (2000). Twentieth century climate change: Evidence from small glaciers. *Proceedings of the National Academy of Science*, **97**(4):1406–1411.

Ekstrand, S. (1996). Landsat TM-based forest damage assessment: Correction for topographic effects. *Photogrammetric Engineering and Remote Sensing*, **62**(2):151–161.

Eliason, P. T., Soderblom, L. A., and Chavez, Jr, P. S. (1981). Extraction of topographic and spectral albedo information from multispectral images. *Photogrammetric Engineering and Remote Sensing*, **48**(11):1571–1579.

Estes, J. E. (ed.) (1983). *Manual of Remote Sensing* (Vol. 2, 2nd edn). Sheridan Press, Falls Church, VA.

Farrand, W. H. (1997). Identification and mapping of ferric oxide and oxyhydroxide minerals in imaging spectrometer data of Summitville, Colorado, U.S.A., and the surrounding San Juan Mountains. *International Journal of Remote Sensing*, **18**(7):1543–1552.

Fily, M., Dedieu, J. P., and Durand, Y. (1999). Comparison between the results of a snow metamorphism model and remote sensing derived snow parameters in the Alps. *Remote Sensing of the Environment*, **68**:254–263.

Finlayson, D. P. and Montgomery, D. R. (2003). Modeling large-scale fluvial erosion in GIS. *Geomorphology*, **53**:147–164.

Flynn, L. P., Harris, A. J., and Wright, R. (2001). Improved identification of volcanic features using Landsat 7 ETM+. *Remote Sensing of the Environment*, **78**:180–193.

Franklin, S. E. and Wilson, B. A. (1992). A three-stage classifier for remote sensing of mountain environments. *Photogrammetric Engineering and Remote Sensing*, **58**(4):449–454.

Gao, J. (2001). Non-differential GPS as an alternative source of planimetric control for rectifying satellite imagery. *Photogrammetric Engineering and Remote Sensing*, **67**(1):49–55.

Gao, X., Sorooshian, S., and Goodrich, D. C. (1993). Linkage of a GIS to a distributed rainfall-runoff model. In: M. F. Goodchild, B. O. Parks, and L. T. Steyaert (eds), *Environmental Modeling with GIS* (pp. 182–187). Oxford University Press, New York.

Giles, P. T. (2001). Remote sensing and cast shadows in mountainous terrain. *Photogrammetric Engineering and Remote Sensing*, **67**(7):833–839.

Goward, S. N. and Williams, D. L. (1997). Landsat and Earth systems science: Development of terrestrial monitoring. *Photogrammetric Engineering and Remote Sensing*, **63**(7):887–900.

Graetz, R. D. (1990). Remote sensing of terrestrial ecosystem structure: An ecologist's pragmatic view. In: R. J. Hobbs and H. A. Mooney (eds), *Remote Sensing of Biosphere Functioning* (pp. 5–30). Springer-Verlag, New York.

Greegor, Jr, D. H. (1986). Ecology from space. *Bioscience*, **36**(7):429–432.

Greuell, W. and de Ruyter de Wildt, M. (1999). Anisotropic reflection by melting glacier ice: Measurements and parametrizations in Landsat TM bands 2 and 4. *Remote Sensing of the Environment*, **70**:265–277.

Gu, D. and Gillespie, A. (1998). Topographic normalization of Landsat TM images of forest based on subpixel sun-canopy-sensor geometry. *Remote Sensing of the Environment*, **64**:166–175.

Haeberli, W. (1998). Historical evolution and operational aspects of worldwide glacier monitoring. In: W. Haeberli, M. Hoelzle, and S. Suter (eds), *Into the Second Century of Worldwide Glacier Monitoring: Prospects and Strategies* (pp. 35–47). UNESCO, Paris.

Haefner, H., Seidel, K., and Ehrler, H. (1997). Applications of snow cover mapping in high mountain regions. *Physical Chemistry of the Earth*, **22**:275–278.

Hall, D. K., Chang, A. T. C., and Siddalingaiah, H. (1988). Reflectances of glaciers as calculated using Landsat-5 Thematic Mapper data. *Remote Sensing of the Environment*, **25**:311–321.

Hall, D. K., Chang, A. T. C., Foster, J. L., Benson, C. S., and Kovalick, W. M. (1989). Comparison of in situ and Landsat derived reflectance of Alaskan glaciers. *Remote Sensing of the Environment*, **28**:23–31.

Hallet, B., Hunter, L., and Bogen, J. (1996). Rates of erosion and sediment evacuation by glaciers: A review of field data and their implications. *Global and Planetary Change*, **12**:213–235.

Halpin, P. N. (1994). GIS analysis of the potential impacts of climate change on mountain ecosystems and protected areas. In: M. F. Price and D. I. Heywood (eds), *Mountain Environments and Geographic Information Systems* (pp. 281–301). Taylor & Francis, London.

Harbor, J. and Warburton, J. (1992). Glaciation and denudation rates. *Nature*, **356**:751.

Holben, B. N. and Justice, C. O. (1981). An examination of spectral band ratioing to reduce the topographic effect of remotely sensed data. *International Journal of Remote Sensing*, **2**:115–123.

Holbo, H. R. and Luvall, J. C. (1989). Modeling surface temperature distributions in forest landscapes. *Remote Sensing of the Environment*, **27**:11–24.

Hook, S. J., Gabell, A. R., Green, A. A., and Kealy, P. S. (1992). A comparison of techniques for extracting emissivity information from thermal infrared data for geologic studies. *Remote Sensing of the Environment*, **42**:123–135.

Howard, A. (1996). The ephemeral mountains. *Science*, **379**:488–489.

Hugli, H. and Frei, W. (1983). Understanding anisotropic reflectance in mountainous terrain. *Photogrammetric Engineering and Remote Sensing*, **49**(5):671–683.

Iqbal, M. (ed.) (1983). *An Introduction to Solar Radiation*. Academic Press, New York.

Isacks, B. L. (1992). Long-term land surface processes: Erosion, tectonics and climate history in mountain belts. In: P. M. Mather (ed.), *TERRA-1: Understanding the Terrestrial Environment* (pp. 21–36). Taylor & Francis, London.

Jacquemoud, S., Bacour, C., Poilvé, H., and Frangi, J. (2000). Comparison of four radiative transfer models to simulate plant canopies reflectance—direct and inverse mode. *Remote Sensing of the Environment*, **74**:471–481.

Kahle, A. B., Madura, D. P., and Soha, J. M. (1980). Middle infrared multispectral scanner data: Analysis for geological applications. *Applied Optics*, **19**:2279–2290.

Kardoulas, N. G., Bird, A. C., and Lawan, A. I. (1996). Geometric correction of SPOT and Landsat imagery: A comparison of map- and GPS-derived control points. *Photogrammetric Engineering and Remote Sensing*, **62**(10):1173–1177.

Kawata, Y., Ueno, S., and Kusaka, T. (1988). Radiometric correction for atmospheric and topographic effects on Landsat MSS images. *International Journal of Remote Sensing*, **9**(4):729–748.

Kimes, D. S. and Kirchner, J. A. (1981). Modeling the effects of various radiant transfers in mountainous terrain on sensor response. *IEEE Transactions on Geoscience and Remote Sensing*, **19**(2):100–108.

Koons, P. O. (1995). Modeling the topographic evolution of collisional belts. *Annual Review Earth and Planetary Science*, **23**:375–408.

Kowalik, W. S., Lyon, R. J. P., and Switzer, P. (1983). The effects of additive radiance terms on ratios of Landsat data. *Photogrammetric Engineering and Remote Sensing*, **49**(5):659–669.

Körner, C. (1994). Impact of atmospheric changes on high mountain vegetation. In: M. Beniston (ed.), *Mountain Environments in Changing Climates* (pp. 155–166). Routledge, London.

Lee, T. J., Pielke, R. A., Kittel, T. G. F., and Weaver, J. F. (1993). Atmospheric modeling and its spatial representation of land surface characteristics. In: M. F. Goodchild, B. O. Parks, and L. T. Steyaert (eds), *Environmental Modeling with GIS* (pp. 108–122). Oxford University Press, New York.

Li, Z. L. and Becker, F. (1993). Feasibility of land surface temperature and emissivity determination from AVHRR data. *Remote Sensing of the Environment*, **3**:67–85.

Lipton, A. E. and Ward, J. M. (1997). Satellite-view biases in retrieved surface temperatures in mountain areas. *Remote Sensing of the Environment*, **60**:92–100.

Luvall, J. C. (1997). The use of remotely sensed surface temperatures from an aircraft-based Thermal Infrared Multispectral Scanner (TIMS) to estimate the spatial and temporal variability of latent heat fluxes and thermal response numbers from a white pine (*Pinus strobus* L.) plantation. In: D. A. Quattrochi and M. F. Goodchild (eds), *Scale in Remote Sensing and GIS* (pp. 169–185). CRC Press, Boca Raton, FL.

Luvall, J. C. and Holbo, H. R. (1989). Measurements of short-term thermal responses of coniferous forest canopies using thermal scanner data. *Remote Sensing of Environment*, **27**:1–10.

Luvall, J. C. and Holbo, H. R. (1991). Thermal remote sensing methods in landscape ecology. In: M. G. Turner and R. H. Gardner (eds), *Quantitative Methods in Landscape Ecology* (pp. 127–152). Springer-Verlag, New York.

Mather, P. M. (ed.) (1992). *TERRA-1: Understanding the Terrestrial Environment*. Taylor & Francis, London.

McClung, D. M. and Armstrong, R. L. (1993). Temperate glacier time response from field data. *Journal of Glaciology*, **39**(132):323–326.

McDermid, G. J. and Franklin, S. E. (1995). Remote sensing and geomorphometric discrimination of slope processes. *Zeitschrift für Geomorphologie*, **101**:165–185.

Meier, M. F. and Dyurgerov, M. B. (2002). How Alaska affects the world. *Science*, **297**:350–351.

Metzger, J. P. and Muller, E. (1996). Characterizing the complexity of landscape boundaries by remote sensing. *Landscape Ecology*, **11**(2):65–77.

Meyer, P., Itten, K. I., Kellenberger, T., Sandmeier, S., and Sandmeier, R. (1993). Radiometric corrections of topographically induced effects on Landsat TM data in an alpine environment. *ISPRS Journal of Photogrammetry and Remote Sensing*, **48**(4):17–28.

Millington, A. C., White, K., Drake, N. A., Wadge, G., and Archer, D. J. (1995). Remote sensing of geomorphological processes and surficial material geochemistry in drylands. In: F. M. Danson and S. E. Plummer (eds), *Advances in Environmental Remote Sensing* (pp. 105–122). John Wiley & Sons, Chichester, UK.

Molnar, P. and England, P. (1990). Late Cenozoic uplift of mountain ranges and global climate change: Chicken or egg? *Nature*, **346**:29–34.

Monteith, J. L. (1973). *Principles of Environmental Physics*. Edward Arnold, London.

Montgomery, D. R. (1994). Valley incision and the uplift of mountain peaks. *Journal of Geophysical Research*, **99**(B7):913–921.

Mysak, L. A., Ingram, R. G., Wang, J., and vanderBaaren, A. (1996). The anomalous sea-ice extent in Hudson Bay, Baffin Bay and the Labrador Sea during three simultaneous NAO and ENSO episodes. *Atmosphere-Ocean*, **34**:313–343.

Nakawo, M., Fujita, K., Ageta, U., Shankar, K., Pokhrel, P. A., and Tandong, Y. (1997). Basic studies for assessing the impacts of global warming on the Himalayan cryosphere. *Bulletin of Glacier Research*, **15**:53–58.

Nellis, M. D. and Briggs, J. M. (1989). The effect of spatial scale on Konza landscape classification using textural analysis. *Landscape Ecology*, **2**(2):93–100.

Norman, J. M., Divakarla, M., and Goel, N. S. (1995). Algorithms for extracting information from remote thermal-IR observations of the Earth's surface. *Remote Sensing of the Environment*, **51**:157–168.

Oke, T. R. (1987). *Boundary Layer Climates* (2nd edn). Methuen, New York.

Palacios-Orueta, A. and Ustin, S. L. (1998). Remote sensing of soil properties in the Santa Monica Mountains. I: Spectral analysis. *Remote Sensing of the Environment*, **65**:170–183.

Palacios-Orueta, A., Pinzón, J. E., Ustin, S. L., and Roberts, D. A. (1999). Remote sensing of soils in the Santa Monica Mountains. II: Hierarchical foreground and background analysis. *Remote Sensing of the Environment*, **68**:138–151.

Pike, R. J. and Park, M. (1995). Geomorphometry—Progress, practice, and prospect. *Zeitschrift für Geomorphologie*, **101**:221–238.

Price, M. F. and Heywood, D. I. (eds) (1994). *Mountain Environments and Geographic Information Systems*. Taylor & Francis, London.

Proy, C., Tanré, D., and Deschamps, P. Y. (1989). Evaluation of topographic effects in remotely sensed data. *Remote Sensing of the Environment*, **30**:21–32.

Quattrochi, D. A. and Goodchild, M. F. (eds) (1997). *Scale in Remote Sensing and GIS*. CRC Press, Boca Raton, FL.

Quattrochi, D. A. and Pelletier, R. E. (1991). Remote sensing for analysis of landscapes: An introduction. In: M. G. Turner and R. H. Gardner (eds), *Quantitative Methods in Landscape Ecology* (pp. 51–76). Springer-Verlag, New York.

Raper, J. and Livingstone, D. (1995). Development of a geomorphological spatial model using object-oriented design. *International Journal of Geographical Information Systems*, **9**(4):359–383.

Raymo, M. E. and Ruddiman, W. F. (1992). Tectonic forcing of the late Cenozoic climate. *Nature*, **359**:117–122.

Raymo, M. E., Ruddiman, W. F., and Froelich, P. N. (1988). Influence of late Cenozoic mountain building on geochemical cycles. *Geology*, **16**:649–653.

Reinking, R. F. (1995). An approach to remote sensing and numerical modeling of orographic clouds and precipitation for climatic water resources assessment. *Forest Ecology and Management*, **35**:349–367.

Richter, R. (1997). Correction of atmosphere and topographic effects for high spatial resolution satellite imagery. *International Journal of Remote Sensing*, **18**(5):1099–1111.

Risser, P. G., Karr, J. R., and Forman, R. T. T. (1984). *Landscape Ecology: Directions and Approaches* (Special Publication No. 2). Illinois Natural History Survey, Champaign.

Robinove, C. J., Chavez, Jr, P. S., and Gehring, D. (1981). Arid land monitoring using Landsat albedo difference images. *Remote Sensing of the Environment*, **11**:133–156.

Rossi, R. E., Dungan, J. L., and Beck, L. R. (1994). Kriging in the shadows: Geostatistical interpolation for remote sensing. *Remote Sensing of the Environment*, **49**:32–40.

Saintot, A., Angelier, J., and Chorowicz, J. (1999). Mechanical significance of structural patterns identified by remote sensing studies: A multiscale analysis of tectonic structures in Crimea. *Technophysics*, **313**(1–2):187–218.

Schmugge, T. J., Kustas, W. P., and Humes, K. S. (1998). Monitoring land surface fluxes using ASTER observations. *IEEE Transactions on Geoscience and Remote Sensing*, **36**(5):1421–1430.

Short, N. M. and Blair, R. W. (eds) (1986). *Geomorphology from Space: A Global Overview of Regional Landforms*. NASA, Washington, DC.

Short, N. M., Lowman, P. D., Freder, S. C., and Finch, W. A. (1976). *Mission to Earth: Landsat Views the World*. NASA, Washington, DC.

Shroder, Jr, J. F. (1989). Hazards of the Himalaya. *American Scientist*, **77**:564–573.

Shroder, Jr, J. F. and Bishop, M. P. (1998). Mass movement in the Himalaya: New insights and research directions. *Geomorphology*, **26**:13–35.

Skelly, W. C., Henderson-Sellers, A., and Pitman, A. J. (1993). Land surface data: Global climate modeling requirements. In: M. F. Goodchild, B. O. Parks, and L. T. Steyaert (eds), *Environmental Modeling with GIS* (pp. 135–141). Oxford University Press, New York.

Skvarca, P., Raup, B., and De Angelis, H. (2003). Recent behaviour of Glacier Upsala, a fast flowing calving glacier in Lago Argentino, Southern Patagonia. *Annals of Glaciology*, **36**:184–188.

Small, E. (1999). Does global cooling reduce relief? *Nature*, **401**:31–33.

Smith, G. R., Woodard, J. C., Heywood, D. I., and Gibbard, P. L. (2000). Interpreting Pleistocene glacial features from SPOT HRV data using fuzzy techniques. *Computers and Geosciences*, **26**:479–490.

Smith, J. A., Lin, T. L., and Ranson, K. J. (1980). The Lambertian assumption and Landsat data. *Photogrammetric Engineering and Remote Sensing*, **46**(9):1183–1189.

Sung, Q. and Chang, T. (2000). Geological interpretation of SPOT imagery: A case study of the Laohushan area in the north Qilian Mountains, NW China. *Geological Society of China*, **43**(1):69.

Tappeiner, U., Tappeiner, G., Aschenwald, J., Tasser, E., and Ostendorf, B. (2001). GIS-based modelling of spatial pattern of snow cover duration in an alpine area. *Ecological Modelling*, **138**:265–275.

Tate, J. N. and Atkinson, P. M. (eds) (2001). *Modelling Scale in Geographical Information Science*. John Wiley & Sons, Chichester, UK.

Teillet, P. M., Guindon, B., and Goodenough, D. G. (1982). On the slope-aspect correction of multispectral scanner data. *Canadian Journal of Remote Sensing*, **8**(2):733–741.

Temps, R. C. and Coulson, K. L. (1977). Solar radiation incident upon slopes of different orientations. *Solar Energy*, **19**:179–184.

Thorne, K., Palluconi, F., Takashima, T., and Masuda, K. (1998). Atmospheric correction of ASTER. *IEEE Transactions on Geoscience and Remote Sensing*, **36**(4):1199–1211.

Turner, M. G. and Gardner, R. H. (eds) (1991). *Quantitative Methods in Landscape Ecology*. Springer-Verlag, New York.

van Westen, C. J. (1994). GIS in landslide hazard zonation: A review, with examples from the Andes of Colombia. In: M. F. Price and D. I. Heywood (eds), *Mountain Environments and Geographic Information Systems* (pp. 135–165). Taylor & Francis, London.

Vermote, E. F., Tanré, D., Deuzé, J. L., Herman, M., and Morcrette, J. (1997). Second simulation of the satellite signal in the solar spectrum, 6S: An overview. *IEEE Transactions on Geoscience and Remote Sensing*, **35**(3):675–686.

Walsh, S. J., Butler, D. R., Brown, D. G., and Bian, L. (1990). Cartographic modeling of snow-avalanche path location within Glacier National Park, Montana. *Photogrammetric Engineering and Remote Sensing*, **56**(5):615–621.

Walsh, S. J., Moody, A., Allen, T. R., and Brown, D. G. (1997). Scale dependence of NDVI and its relationship to mountainous terrain. In: D. A. Quattrochi and M. F. Goodchild (eds), *Scale in Remote Sensing and GIS* (pp. 27–55). CRC Press, Boca Raton, FL.

Wan, Z. and Dozier, J. (1989). Land-surface temperature measurements from space: Physical principles and inverse modeling. *IEEE Transactions on Geoscience and Remote Sensing*, **27**:268–277.

Welch, R., Jordan, T., Lang, H., and Murakami, H. (1998). ASTER as a source for topographic data in the late 1990's. *IEEE Transactions on Geoscience and Remote Sensing*, **36**(4):1282–1289.

Whipple, K. X., Kirby, E., and Brocklehurst, S. H. (1999). Geomorphic limits to climate-induced increases in topographic relief. *Nature*, **401**:39–43.

Williams, R. S. and Ferrigno, J. G. (eds) (1989). *Satellite Image Atlas of Glaciers of the World*. U.S. Geological Survey, Denver, CO.

Williams, R. S., Hall, D. K., and Benson, C. S. (1991). Analysis of glacier facies using satellite techniques. *Journal of Glaciology*, **37**(125):120–128.

Yang, C. and Vidal, A. (1990). Combination of digital elevation models with SPOT-1 HRV multispectral imagery for reflectance factor mapping. *Remote Sensing of the Environment*, **32**:35–45.

Michael P. Bishop and John F. Shroder, Jr

Geographic Information Science and Mountain Geomorphology

Springer

Published in association with
Praxis Publishing
Chichester, UK

PRAXIS

Dr Michael P. Bishop and Dr John F. Shroder, Jr
Department of Geography and Geology
University of Nebraska at Omaha
Omaha
USA

SPRINGER–PRAXIS BOOKS IN GEOPHYSICAL SCIENCES
SUBJECT *ADVISORY EDITOR*: Dr Philippe Blondel, C.Geol., F.G.S., Ph.D., M.Sc., Senior Scientist, Department of Physics, University of Bath, Bath, UK

ISBN 3-540-42640-X Springer-Verlag Berlin Heidelberg New York

Springer-Verlag is a part of Springer Science+Business Media (springeronline.com)
Bibliographic information published by Die Deutsche Bibliothek
Die Deutsche Bibliothek lists this publication in the Deutsche Nationalbibliografie; detailed bibliographic data are available from the Internet at http://dnb.ddb.de

Library of Congress Cataloging-in-Publication Data
Geographic information science and mountain geomorphology /
[edited by] Michael P. Bishop and John F. Shroder, Jr.
p. cm.
Includes bibliographical references.
ISBN 3-540-42640-X (alk. paper)
1. Mountains. 2. Geographic information systems. 4. Geomatics.
I. Bishop, Michael P., 1958– II. Shroder, John F., 1939–
GB501.2.G465 2004
551.43—dc22 2003063350

Cover design: Jim Wilkie
Project Management: Originator Publishing Services, Gt Yarmouth, Norfolk, UK

Printed on acid-free paper